Journal of Structural Geology 31 (2009) 1039–1057

Contents lists available at ScienceDirect

Journal of Structural Geology

journal homepage: www.elsevier.com/locate/jsg

Conditions during syntectonic vein formation in the footwall of the Absaroka Thrust Fault, Idaho–Wyoming–Utah fold and thrust belt

David V. Wiltschko*, George R. Lambert, Will Lamb

Department of Geology and Geophysics, Center for Tectonophysics, Texas A&M University, College Station, TX 77843-3113, USA

ARTICLE INFO

Article history:
Received 28 November 2007
Received in revised form
10 September 2008
Accepted 12 March 2009
Available online 24 March 2009

Keywords:
Veins
Fluids
Thrust faults
Idaho–Wyoming thrust belt
Deformation
Twin Creek Limestone
Fractures
Stable isotopes
Fluid inclusion
Calcite strain gauge

ABSTRACT

The Twin Creek Limestone in the footwall of the Absaroka thrust sheet contains three sets of bed-normal syntectonic calcite veins. Vein formation occurred during Cretaceous motion along the Absaroka thrust fault as indicated by (1) crosscutting relationships among these vein sets, (2) a previously dated solution cleavage, and (3) calcite twin analysis. Fluid inclusions in the veins and overburden estimates constrain inclusion entrapment temperatures to be between 175 °C and 328 °C. Results from stable oxygen isotopes indicate that the host and vein fluid compositions were in near isotopic equilibrium. Applying both reasonable geothermal gradients and constraints on overburden temperature yields fluid pressures during vein precipitation that are near hydrostatic. All data taken together suggest both that vein formation within the Twin Creek Formation occurred in a relatively closed system, and that the veins filled near hydrostatic fluid pressure. Because the veins fill precursory cracks, vein filling might not reflect the maximum fluid pressure that existed during the complete vein forming process.

1. Introduction

Although abnormal fluid pressures have been invoked to explain the apparent weakness of both thrust fault zones and thrust wedges (e.g. Hubbert and Rubey, 1959; Davis et al., 1983; Dahlen et al., 1984), direct evidence for abnormal fluid pressure in ancient continental margin thrust belts is sparse (e.g. Yonkee et al., 1989; Montomoli et al., 2001; O'Hara and Haak, 2002; Montomoli et al., 2005; Mazzarini and Isola, 2007). Several arguments and lines of indirect evidence have generally been used to infer the existence of abnormally high fluid pressures in ancient thrust belts. The first is uniformitarianism. Drilling records from the Taiwan fold and thrust belt as well as other active accretionary prisms confirm that abnormally high fluid pressures exist in this tectonic setting at present (e.g., Suppe and Wittke, 1977; Moore et al., 1982). The inference is that accretionary prisms and continental margins undergoing contraction are sufficiently similar so that processes occurring now in the former probably occurred in the past in the latter. The second is vein studies. The presence of syntectonic veins may indicate that fluid pressures were high at the time of their formation because abnormal fluid pressure is needed to lower the driving stress required to open and propagate fractures (e.g. Segall and Pollard, 1983; Pollard and Segall, 1987; Olson and Pollard, 1991). To the extent that veins are hydrofractures, data from both their shapes and fluid inclusions contained within the vein fillings may provide information on the fluid pressure during vein formation. In addition, the compositions of syntectonic veins have been studied by a variety of means to understand the fluid source and composition (e.g. Rye and Bradbury, 1988; Erel and Katz, 1990; Bottomley and Veizer, 1992; Shemesh et al., 1992). These studies have shown that small scale cross and longitudinal variations in trace metals and stable isotopes of both oxygen and carbon may be preserved. The veins may also preserve minerals that precipitated from fluids in equilibrium with rock of composition significantly different from the local host (e.g., Rye and Bradbury, 1988; Erel and Katz, 1990); the fluid sources for veins of different generations may also be determined (Gao et al., 1992; Shemesh et al., 1992). In some cases, closed system conditions seem to better match the data (Teufelin, 1994).

Fluid inclusions within syntectonic veins have also been examined to place constraints on fluid pressure at the time of veining (e.g., Srivistava and Engelder, 1990; Foreman and Dunne,

* Corresponding author.
E-mail address: wiltschko@geo.tamu.edu (D.V. Wiltschko).

0191-8141/$ – see front matter © 2009 Elsevier Ltd. All rights reserved.
doi:10.1016/j.jsg.2009.03.009

1991; Montomoli et al., 2001, 2005). The large pressure range displayed by these data—between what one would expect from lithostatic and hydrostatic thermobaric gradients—exists in part because both the burial and uplift history and timing of vein formation are poorly understood. Studies that rely on fluid inclusions alone are usually hampered by a lack of independent knowledge of the depth of burial unless complex fluid inclusion fillings provide further constraints. Without independent knowledge of depth, it is not possible to determine whether or not a measured fluid pressure is abnormal.

The purpose of this study is to constrain the range of fluid pressure values that existed in the footwall of the Idaho–Wyoming–Utah fold and thrust belt of the Absaroka thrust fault during deformation. We have coupled microthermobarometric and stable isotopic geochemistry to place constraints on the fluid source and pressure during thrusting in an area where there is some constraint on the depth of burial. The argument we make is that (1) the veins in our study are syntectonic, (2) the fluid source for the veins was from within the local host and thus, (3) thermal maturity studies and oxygen isotopes may be used to constrain the geothermal gradients in the region and then place these particular rocks occupied in pressure–temperature space. With these constraints and important assumptions discussed below, we have a fluid pressure (P_f) from fluid inclusions.

1.1. Regional geology

The fold and thrust belt of western Wyoming and southeastern Idaho forms an arcuate belt approximately 300 km long and 100 km wide, extending from the Snake River Plain southward into Utah. The belt is concave toward the west and is cut by six major thrust faults, many minor thrust faults, and late normal faults (Armstrong and Oriel, 1965; Royse et al., 1975). From west to east, the major thrust faults include the Paris, Meade, Crawford, Absaroka, Darby, and Prospect faults (Fig. 1). Thrusting in this portion of the belt occurred during the early Cretaceous through early Eocene time (e.g. Armstrong and Oriel, 1965; Wiltschko and Dorr, 1983; DeCelles, 1994). The sequence of the thrust initiation was generally from west (hinterland) to east (foreland). The time of first motion of the major thrust faults is apparently earlier to the east, although there are out of sequence motions (Lamerson, 1982). Initial motion on the Mead thrust was dated by DeCelles et al. (1993) as 118–113 Ma (Aptian). The Crawford thrust is dated as 84–86 Ma (Coniacian–Santonian; see discussion in Wiltschko and Dorr, 1983; DeCelles, 1994). Slip on the Absaroka thrust fault (Fig. 1) began about 83 Ma (Campanian) and continued until 62 Ma during the Maastrichtian (Jacobson and Nichols, 1982). Although more difficult to date, the Darby thrust moved about 61 Ma (Torrejonian).

The thrust belt has been undergoing Basin and Range related extension since the Eocene (Royse et al., 1975; Wiltschko and Dorr, 1983; Anders et al., 1989). Large Tertiary normal faults bound many of the north-south valleys, such as Star Valley and Grand Valley (Fig. 1; Rubey, 1973; Oriel and Platt, 1980). The normal faults forming these half-grabens are generally interpreted to flatten with depth and join with the Absaroka thrust (Royse et al., 1975; Dixon, 1982). However, the quality of published seismic data is not good enough to rule out their cutting basement.

1.2. Local geology

The study area is located in the footwall of the Absaroka thrust sheet, 3.4 km east of the exposed trace of the thrust (Fig. 2). Two outcrops of Twin Creek Limestone located on a hillside due east of the confluence of Lookout Creek and the Grays River were selected for this study. The present strike of bedding within the Twin Creek

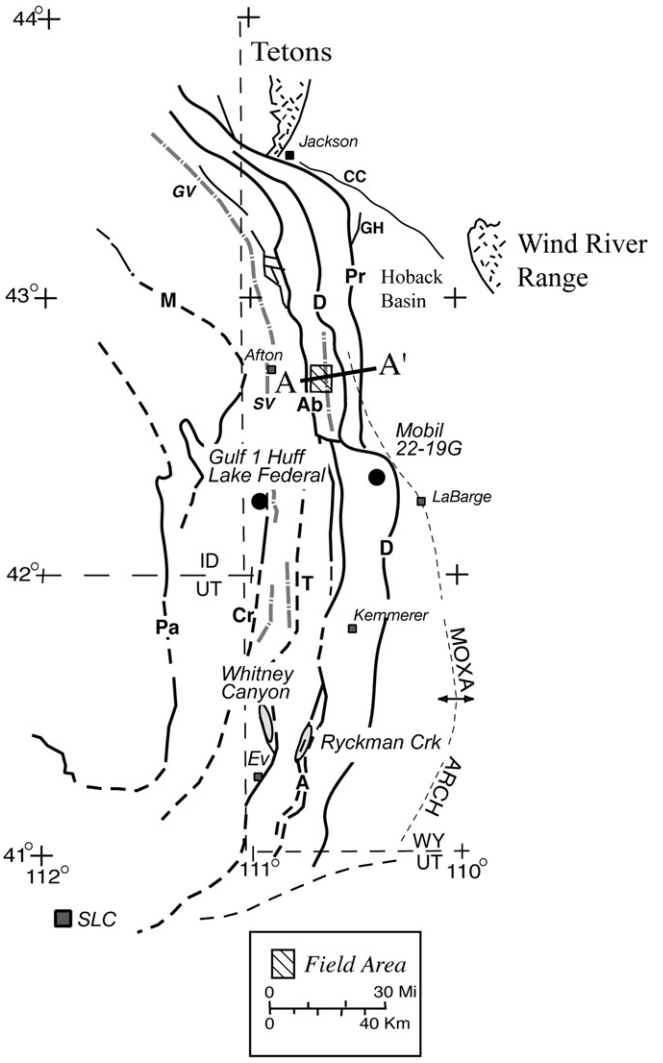

Fig. 1. Tectonic map of the Idaho–Wyoming–Utah fold and thrust belt, after Royse et al. (1975). The cross-hatched box represents the location of the study area. Solid or simple dashed lines are thrust or reverse faults and dot-dash gray lines are normal faults. Pa, Paris thrust; M, Meade thrust; Cr, Crawford thrust; A, Absaroka thrust; T, Tunp thrust; D, Darby thrusts; Pr, Prospect thrust; CC, Cache Creek fault; GH, Game Hill fault; GV Grand Valley fault; SV Star Valley fault; SLC, Salt Lake City, Utah; Ev, Evanston Wyoming. Whitney Canyon and Ryckman Creek (shaded) are two petroleum fields discussed in the text (from Warner and Royse, 1987).

Formation (N4E 35NW) is roughly perpendicular to the west-to-east transport direction of the Absaroka thrust sheet, determined from minor structures. Therefore, the transport direction is nearly due east. Large-scale folding or faulting is absent within a 2.5 km radius of this area (Fig. 2). The Grays River normal fault lies to the east of our study site. Although its geometry is not known, we interpret is to be a late reactivation of a ramp in the Darby thrust.

The Twin Creek formation was selected at this site for several reasons: (1) it is a veined carbonate, (2) it is close to the exposed Absaroka thrust fault, (3) it crops out in dip slopes, and (4) it lies in simpler structural setting than the poorly exposed fault zone (Fig. 3).

1.3. Twin Creek Formation

The Twin Creek Formation is a middle to upper Jurassic shallow marine sequence and is considered equivalent to the lower Sundance Formation of the Black Hills (Wanless et al., 1955). The Twin Creek Formation is composed of resistant ledge-forming

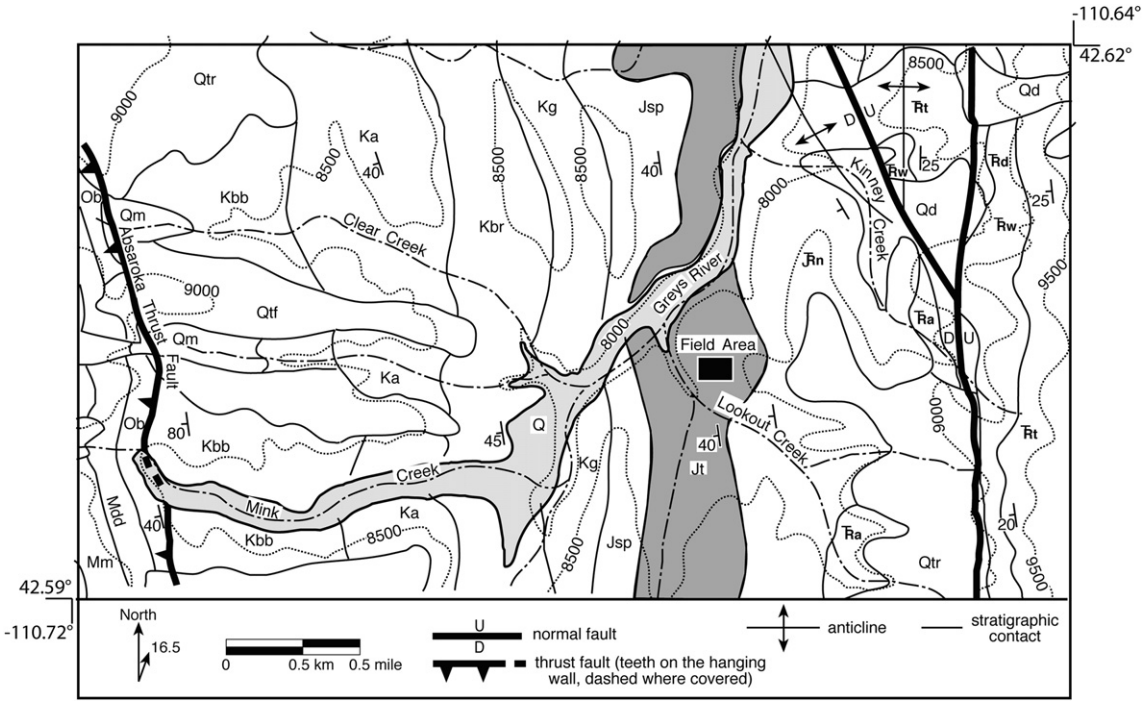

Fig. 2. Field area map after Rubey (1973). Dark shading is the outcrop belt of the Jurassic Twin Creek Limestone.

limestones (Twin Creek Limestone) and interbedded argillaceous intervals. The argillaceous units are light gray, hard, and calcareous (Wanless et al., 1955). The limestones are oölitic, bioclastic and/or micritic, dark gray and laterally discontinuous over large areas. The oöid size, where present, is variable, and the matrix is dominantly micrite with minor amounts of authigenic quartz. The limestone-dominant sections within the Twin Creek Formation contain thin (<3 cm) argillaceous interbeds. The limestone beds mapped in this study range in thickness from 30 to 60 cm as measured from the exposed bedding surface of the outcrop to the depth of the first shale interbed encountered. The overall stratigraphic thickness of the Twin Creek Formation in the field area is approximately 435 m. The outcrops selected for this study are located in the middle of the formation, approximately 200 m above the base.

2. Field methods and observations

Features mapped on the outcrops include calcite veins, solution cleavages, and fractures (Fig. 4). All features were mapped at 1:12 and several vein arrays were mapped at 1:6 for greater detail (Figs. 5–7).

Solution cleavage surfaces are all bed-normal and have the same N5W trend in all outcrops (Fig. 8a). Solution cleavage surfaces are stained orange-brown and appear as wavy raised traces on the outcrop surface due to their greater resistance to weathering. Many solution cleavage surfaces branch and intersect each other at low angles (Fig. 5; station 1). Lengths range from a few centimeters to tens of centimeters. Thicknesses of these features are always less than 2 mm.

Although a variety of open fracture (joint) orientations exist in the field area, two dominant trends (N5W and N70E) are present (Fig. 8b). All fractures are normal to bedding and lack any measurable shear offset in outcrop.

Calcite veins have been grouped into one of three categories based on their average trend (Fig. 8c). Like the fractures, all three vein types are bed-normal. The two common vein trends are transport-parallel veins and N65E veins (Fig. 8c). A third rare N40W striking type is also present. All vein types (1) have sharp boundaries with the host rock, (2) contain in hand sample a blocky calcite fabric that lacks internal zoning, and (3) are more resistant to weathering than the host rock. Veining is contained within limestone beds; we observed no significant veining in the argillaceous layers. There are no bedding parallel veins; the observed shale/limestone contacts also lack mineralization.

En echelon arrays of transport-parallel veins (N85W) are the dominant type of veining present in all outcrops examined. Most

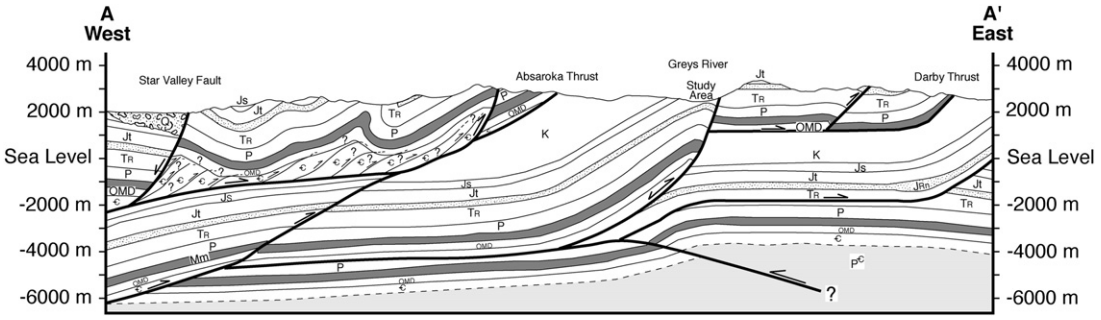

Fig. 3. Cross section. Surface geology from Rubey (1973). Line of section is A–A′ on Fig. 1. K, Cretaceous, undivided. Js, Stump and Preuss Formations. Jrn, Jurassic Nugget Formation. Tr, Triassic, undivided. P, Permian Phosphoria Formation. Mm, Mississippian Madison Group. OMD, Ordovician through Devonian, undivided. Depth to basement from Dixon (1982).

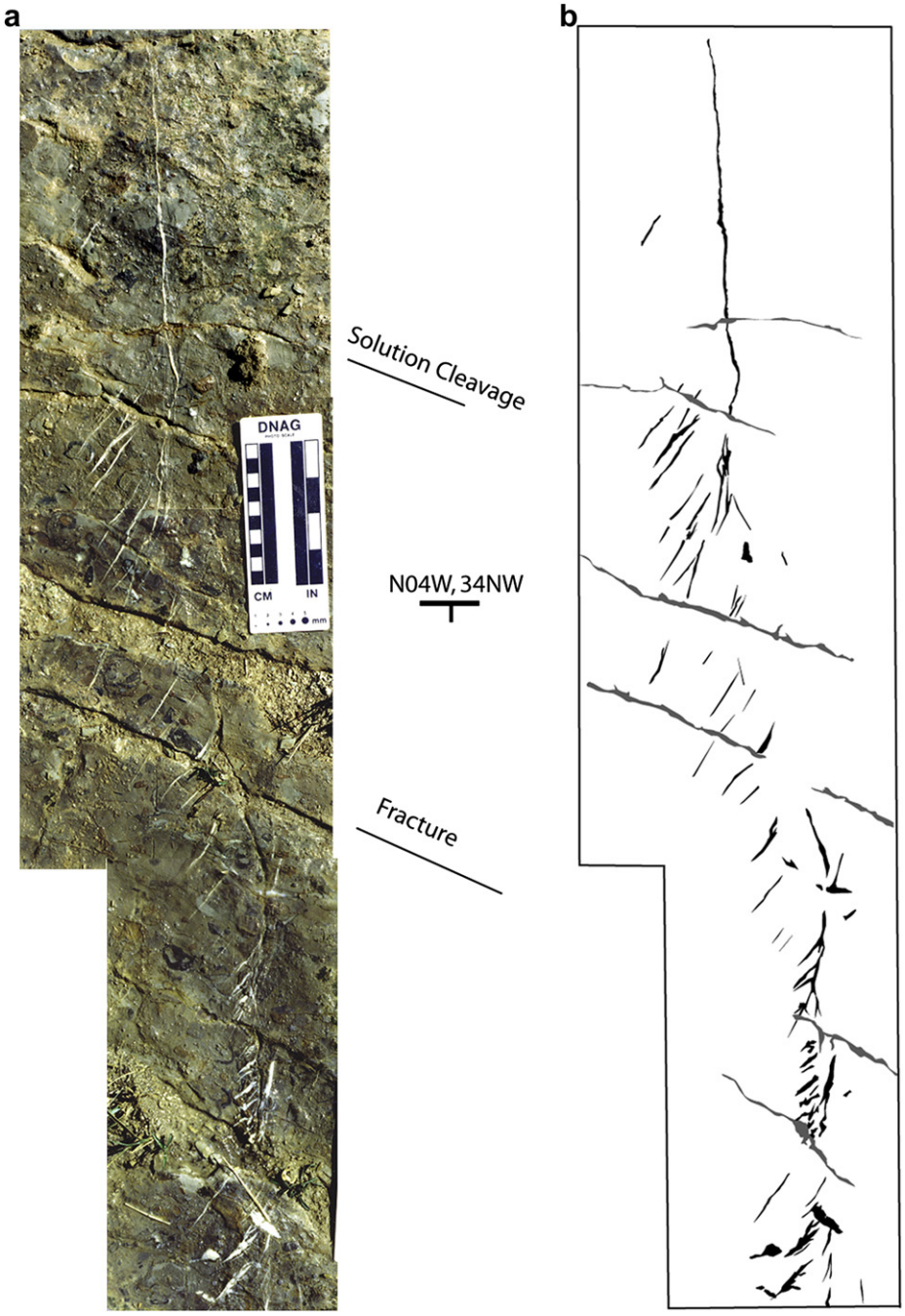

Fig. 4. Photomosaic (a) and line drawing (b) of a bedding surface in the Twin Creek Limestone illustrating the mapped outcrop fabrics. Strike and dip symbol indicates the orientation of bedding. (b) Light gray pattern for solution cleavage surfaces and fractures, black for veins.

transport-parallel veins are composed of white calcite, but a few contain traces of an orange-brown fine grained substance which is optically unresolvable in standard 30 μm thin sections. This orange substance was revealed to be ferroan calcite by X-ray diffraction and microprobe analysis. Transport-parallel veins are mainly in left-stepping en echelon array systems (Fig. 5; station 2) with an average array trend of N65E (Fig. 8d). Markers in the host rock and on opposite vein walls indicate that no significant shear motion associated with the formation of these en echelon array patterns has occurred. Veins within arrays do not merge into a parent fracture or vein at depth. Array lengths range from less than one to four meters. Both the measured spatial parameters and individual geometry of transport-parallel veins are discussed in greater detail below.

N65E veins are bed normal and strike parallel to the trend of the en echelon arrays of the transport-parallel veins. They occur as isolated veins, but are sometimes located near transport-parallel vein tips. Some N65E veins cross-cut and link transport-parallel vein tips (Fig. 5; station 3).

N40W veins are composed of orange blocky calcite. These veins have a wavy surface trace along their trend when compared to the relatively straight trends of the other vein types (Fig. 5; station 4). Less than ten N40W veins are present in the mapped areas.

2.1. Transport-parallel vein geometry

Measurements were made on 37 transport-parallel veins from seven vein arrays. Data were obtained from both field measurements

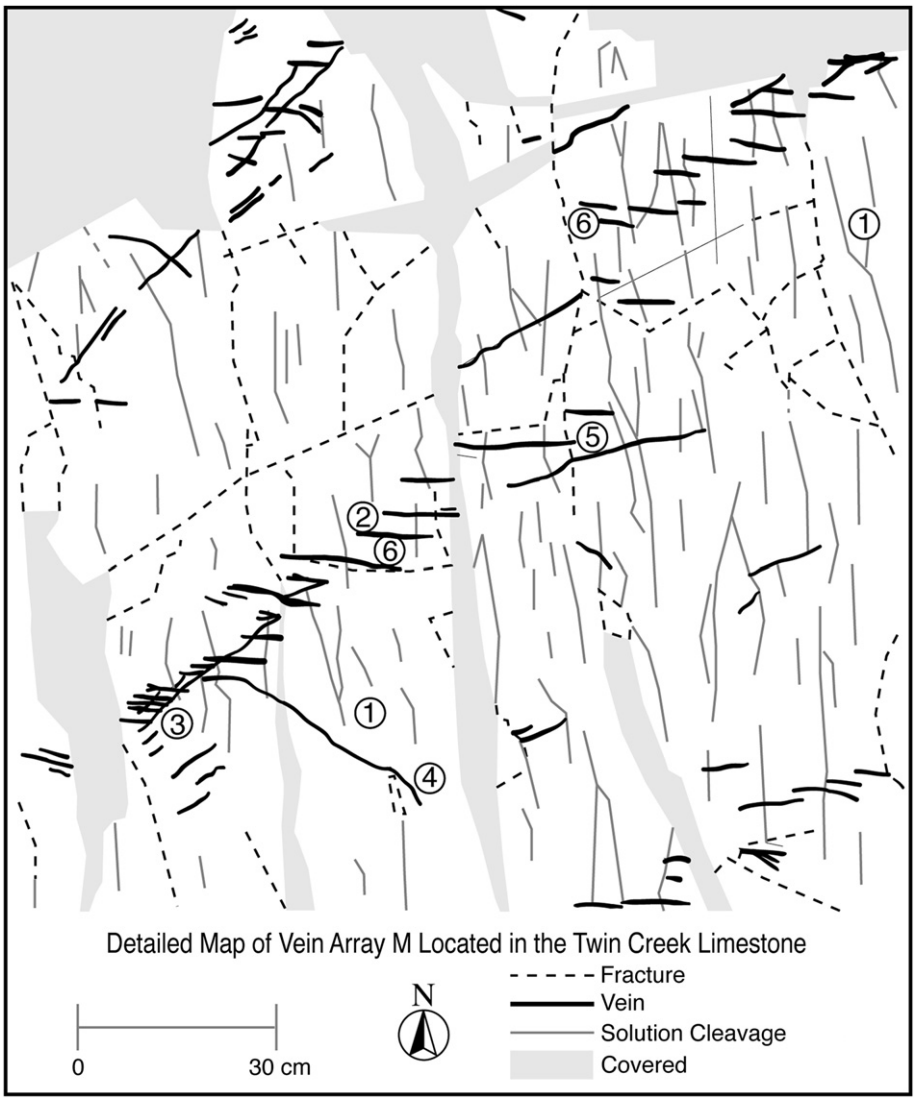

Fig. 5. Detailed map of all typical Twin Creek Limestone outcrop fabrics. Field stations (1–6) are discussed in the text. The orientation of the transport direction for the Absaroka thrust sheet is from west to east. Mapped at 1:6.

and measurements obtained from large-scale field maps (e.g., Figs. 6 and 7). All parameters recorded from outcrop maps, except vein width, are accurate to ±2.0 cm when results are compared against values measured on the same veins in the field. These measurements included: length (L), width (W) at the mid point, spacing (S), and overlap (O) (Fig. 9). The parameters of vein array angle (δ), and vein array position (P) (Fig. 9) were also obtained from the field maps. Vein length was only measured if both vein tips were observed. Vein widths have a lower limit bias of 1 mm. The spacing, overlap, array angle, and vein position were measured between the first transport-parallel vein (westernmost observed vein in the array) and the nearest neighbor to the left in all left stepping arrays (Fig. 9).

2.2. Vein shape

Transport-parallel veins are generally straight, lacking significant curvature at their tips (Fig. 5; station 6). However, a few veins do contain small terminal forks (Beach, 1977) (Fig. 5; station 5). There is a weak linear relationship between vein length and width, suggesting that longer veins are more dilated (Fig. 10a).

2.3. Spatial relationships

Researchers have suggested that a correlation exists between individual crack dimensions and the location of the nearest neighboring crack (Beach, 1975; Pollard et al., 1982; Nicholson and Pollard, 1985; Pollard and Aydin, 1988; Olson and Pollard, 1989, 1991). An isolated crack in a favorable orientation for a given stress state will open and grow longer compared to closely spaced or overlapping cracks with the same orientation. However, a comparison of transport-parallel vein spacing versus vein width (Fig. 10b), and an analysis of vein tip overlap versus vein spacing, shows no such correlation (Fig. 10c). Comparing vein spacing against vein array angle produces a significant linear relationship ($R = 0.5$) suggesting that the spacing/length (S/L) ratio increases as the array angle decreases (Fig. 10d). A similar weak trend may exist for width/length and array angle (Fig. 10e). A linear relationship also results when overlap is compared to array angle (Fig. 10f) suggesting that as the amount of overlap increases, the array angle may increase. A weak comparison of vein width versus vein position suggests the widest veins/cracks occur towards the middle portion of arrays (Fig. 10g). Although a plot of normalized spacing (S/L)

Fig. 6. Outcrop map, 1:12. See text for discussion.

versus width (Fig. 10b) produced no definitive trend, comparisons of vein spacing versus length (Fig. 10h) and spacing versus width (Fig. 10i) suggest that with increased vein spacing, individual vein length and width also increase.

These data may be used in conjunction with fracture mechanics to place constraints on the driving stress that may have been present during vein formation. Propagation of an isolated Mode I crack in a linear elastic medium is directly related to the fracture opening displacement. For example, the width to length ratio (W/L) of a uniformly loaded Mode I fracture is given by

$$W/L = \frac{2\left(P_f - \sigma_3\right)\left(1-\nu^2\right)}{E} \tag{1}$$

where $P_f - \sigma_3$ is the driving stress, or difference between fluid pressure, P_f, and σ_3 the normal stress acting on the fracture walls, and ν and E are the Poisson's ratio and Young's modulus, respectively (e.g., Jaeger and Cook, 1979; Pollard and Aydin, 1988). This equation allows the calculation of the driving stress present during propagation provided that (1) the material is linear elastic, (2) values of the elastic moduli can be estimated for the depth and time of fracturing, and (3) the opening displacement value is the true amount of opening displacement (one crack event) and not a summation of multiple cracking events. The elastic properties of the Twin Creek at the time and depth of deformation are not known. However, they may be estimated using V_s and V_p velocities measured in the Twin Creek Limestone. Parra et al. (1999) report seismic velocity data for the Twin Creek from the Lodgepole Field in the southwest portion of the Idaho–Wyoming–Utah thrust belt. The upper and lower limits are 2.67 and 3.04 km/s for V_s and 5.28 and 6.03 km/s for V_p, respectively. Using these values and the well-known relationships

$$V_s = \sqrt{\frac{\mu}{\rho}}$$
$$V_p = \sqrt{\frac{k+\frac{4\mu}{3}}{\rho}} \tag{2}$$

where k and μ are the bulk and shear moduli, respectively, and ρ is density. Solving for k and μ and converting to E and ν, using

$$E = \frac{9k\mu}{3k+\mu}$$
$$\nu = \frac{3k-2\mu}{2(3k+\mu)} \tag{3}$$

then Poisson's ratio is 0.33 and the upper to lower bounds for Young's modulus are 50.2 to 68.8 GPa. From Fig. 10, the average outcrop aperture to length ratio of the veins averages about 0.05. This yields a driving stress of between 1410 and 1930 MPa. If σ_3 is the overburden stress, then these values imply a fluid pressure in excess of the overburden stress. However, many veins show multiple generations of cracking in thin section with a typical fracture width of about 10 μm (e.g., Fig. 11b). Although we have no values for the length of each one of these fractures, if we assume that each spans the entire length of the vein, then the fluid pressure required is between 281 and 386 MPa. These values are most likely the lower values under the assumptions made.

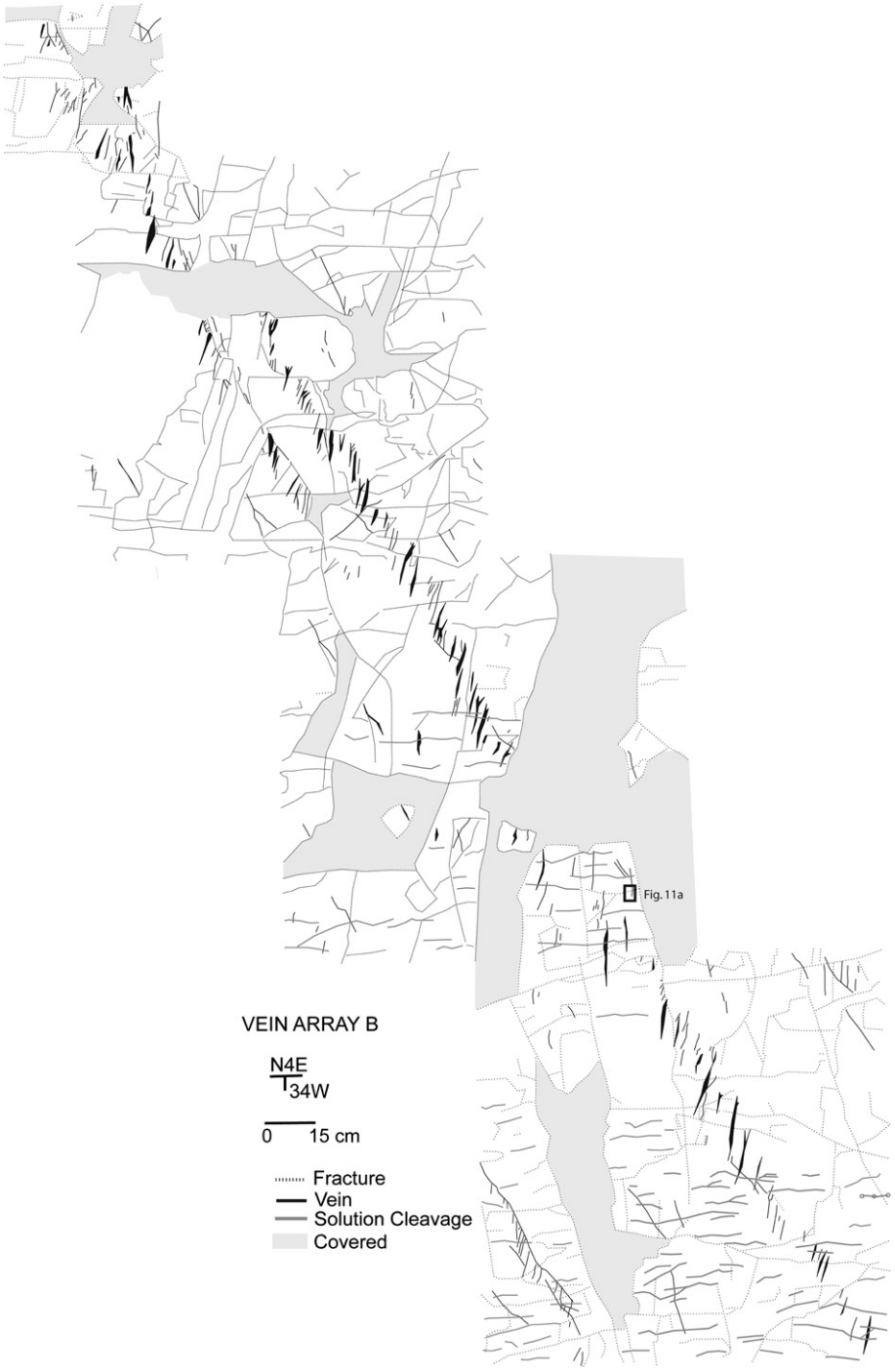

Fig. 7. Vein array maps, 1:6. Small rectangle: location of Fig. 11a. See text for discussion.

The N85W veins occur in en echelon arrays and the calculated driving stress related to the propagation of these Mode I cracks will be larger than the value calculated for an isolated Mode I crack due to mechanical interaction between neighboring fracture tips (e.g., Pollard et al., 1982; Olson and Pollard, 1991). As the number of veins in an array increases, the relative dilation difference between the last crack in an array and an isolated crack approaches zero. Thus, the driving stress calculated for the last member of en-echelon vein array will approach the value for an isolated Mode I crack as the number of array cracks increases.

A comparison between the measured N85W vein spatial parameters and spatial parameters from numerical models of fracture may provide a measure of the propagation energy G required for the formation of en-echelon arrays of N85W veins (Olson and Pollard, 1991). Unfortunately, all results from numerical models are reported normalized to the propagation ratio G/G_I where G_I equals the propagation energy for an isolated crack of the same length as a middle array crack a five-member array. This relationship cannot be calculated for the naturally occurring N85W vein arrays. Thus, a measure of the propagation force G for the N85W vein arrays cannot be determined. However, the intersection of the average N85W vein array angle ($\delta = 40$) and the average N85W vein S/L ratio of 0.5 would occur above the G/G_I value of one. This suggests that propagation of the

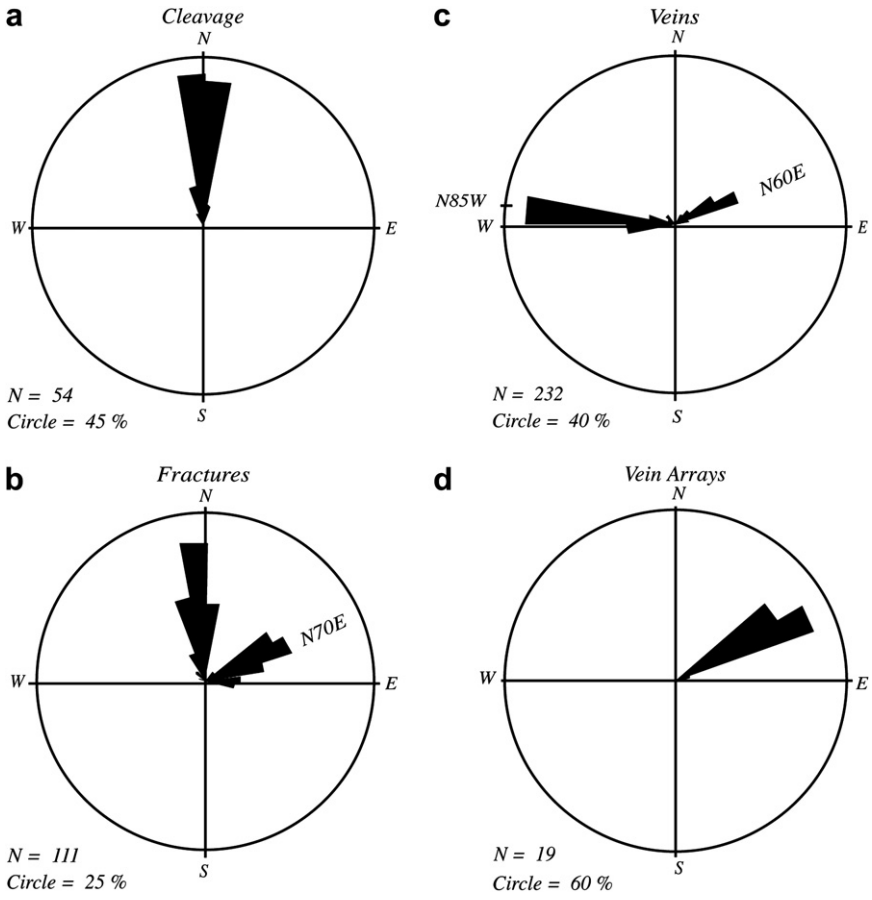

Fig. 8. Rose diagrams illustrating trends of all outcrop fabrics. (a) Solution cleavages, (b) fractures, (c) calcite veins, (d) left-stepping en echelon arrays.

N85W veins and the formation of the en echelon arrays were enhanced by mechanical fracture interaction. Moreover, the propagation paths of the overlapped regions of the N85W en-echelon veins remain relatively unchanged (see Figs. 6, 7). This suggests that the magnitude of stress acting parallel to the fractures was large compared to the magnitude of the driving stress.

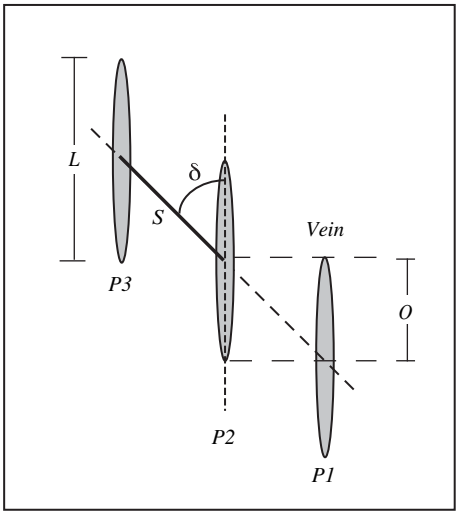

Fig. 9. Spatial and geometric parameters associated with N85W veins. δ, vein array angle; *S*, vein spacing; *L*, vein length; *O*, vein overlap; *P*, vein array position. Vein width (*W*) is measured at the mid-point of each vein.

2.4. Vein petrology

Mutually perpendicular 30 μm-thick thin sections from each vein type were examined using both cathodoluminescence (CL) and polarized and plane light (PPL). Transport-parallel and N65E veins display the same dull orange luminescence as the host. N40W veins contain a mix of regions, some areas with similar luminescence as the host and other patchy isolated non-luminescent regions. Zonation parallel to the vein walls interface was absent in all vein types examined under both CL and PPL.

The dominant mineralogy of all vein types is calcite, although a few veins contain randomly distributed dolomite and quartz crystals. Calcite fillings in all vein types are largely composed of subhedral calcite crystals. Although the size and crystallographic orientation of calcite crystals within an individual vein are variable (Fig. 11a), the largest vein calcite crystals are generally located in the widest veins. A systematic increase in crystal size from the host/vein interface towards the vein center is not common, although some veins display a change in crystal size (Fig. 11c, pt 2). Vein calcite crystals are generally larger than calcite grains within the host (Fig. 11c). However, the smallest veins often display overgrowths on host grains (Fig. 11b). These same veins are composed of bands of host inclusions ranging in size from a few microns to a few mm. All vein types contain twinned calcite grains and small ($<$4 μm diameter) fluid inclusions. Microscopic analysis of mutually perpendicular thin sections for all vein types show vein walls to be relatively smooth mirror images of each other lacking any shear offset (Fig 11c, pt 1). En passant fracture interactions are common (Fig. 11a). Several transport-parallel and N65E veins contain a central

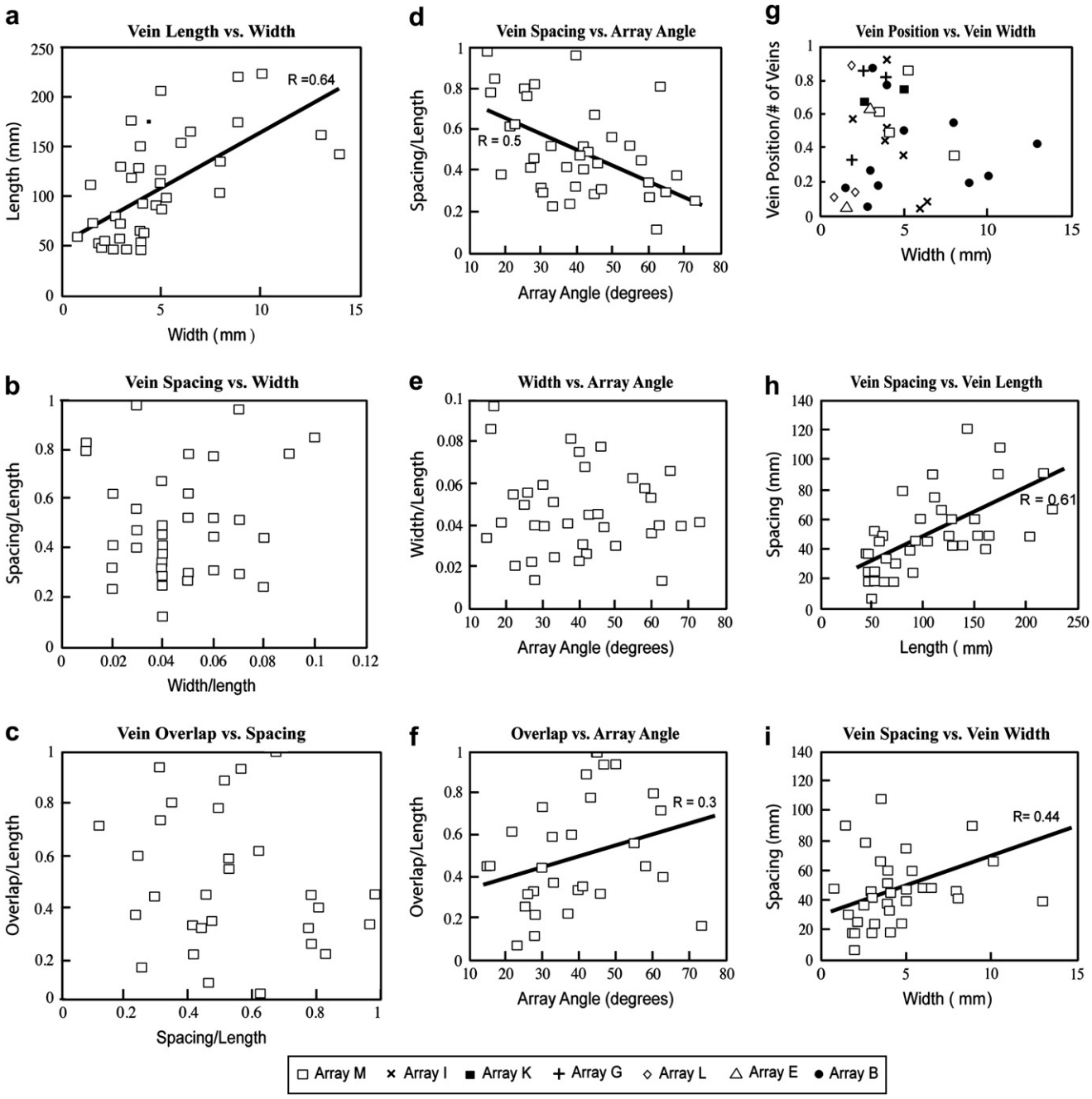

Fig. 10. Geometric and spatial comparisons of N85W veins. Solid lines represent a best fit for the given data.

parting (Fig. 11c). When present, the parting is defined by a zone of smaller calcite crystals. CL properties of the sub-vein are the same as the primary vein. Late shear zones are also located near the center of several individual veins. (Fig. 11c, pt 3). These shear zones are characterized by decreased grain size and anastomosing shear surfaces. The amount of offset is small in the plane of bedding.

2.5. Timing of vein formation

Although all outcrop features, excluding open fractures, may be related to the same tectonic event, a sequence of events has been established using the relative abundance of various cross-cutting relationships. The formation of solution cleavage surfaces and transport-parallel veins is synchronous based on the fact that transport-parallel veins and solution cleavage surfaces cross-cut each other. This cross-cutting relationship is observed at both the outcrop and thin section scales and has also been reported at other locations within the Twin Creek Formation (Mitra et al., 1984). A weak argument may be made for N65E veining to have occurred slightly later, both because fewer solution cleavage surfaces were found cross-cutting these veins and several N65E veins link and cross-cut transport-parallel vein tips (Fig. 5; station 3). Although the timing relationship between N40W veins and solution cleavage surfaces is unclear, N40W veins cross cut all other vein types and are interpreted to represent the last episode of veining. The open fractures cross-cut all other features, and thus they are interpreted as the youngest deformation feature present, perhaps as a result of uplift and dissolution.

The formation of solution cleavage surfaces in the Twin Creek Formation is thought to be synchronous with Cretaceous—aged

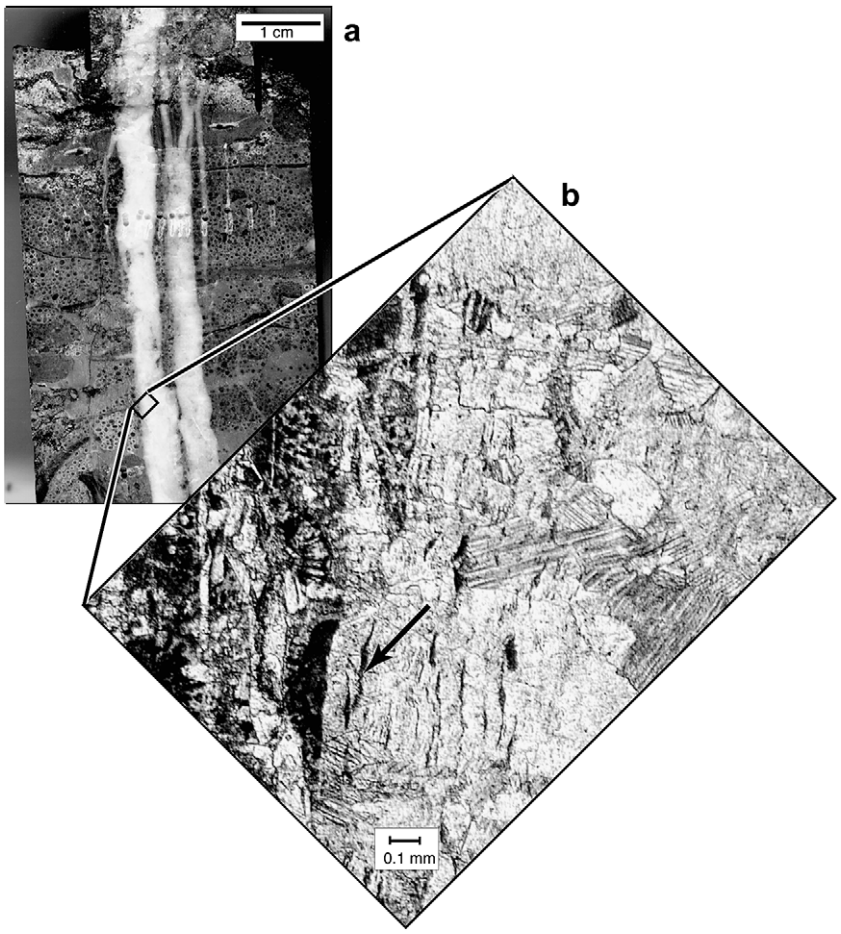

Fig. 11. Photomicrographs of Twin Creek Limestone vein fabrics. The orientation of all photo micrographs is parallel to bedding. (a) Photograph of chip (RL2201); see Fig. 7 for location. (b) Thin section, plane light. Note numerous host inclusions (arrow). (c) Blocky calcite fill of vein showing en passant fracture geometry (RL401). (d) Banded vein fabric (RL1501). 1, ooid cut by small vein splay without shear offset; 2, host inclusions in banded vein; 3, crystal orientation mimicked across the vein; e, large sheared vein (RL1701). 1, smooth vein wall with columnar calcite crystals; 2, transition to fine grained, blocky calcite; 3, shear zone marking the center of vein<comment>Fig. 11: Please check that legend and text correspond to illustrations provided (part 1a, b; part 2a, b, c)</comment>.

compression associated with motion along the Absaroka thrust fault (Mitra et al., 1984). The evidence is that Cretaceous Echo Canyon, Little Muddy Creek, and Lookout Mountain synorogenic conglomerates contain Twin Creek micrite clasts with cleavage (Gentry, 1983). This cleavage is developed at high angles to the bedding within the clasts and shows no relationship to the local structure containing the synorogenic deposits (Mitra et al., 1984). Cleavage is also absent in the matrix of the conglomerate. The synchronous cross-cutting relationship between the syntectonic veins and the solution cleavage surfaces within the Twin Creek Formation of this study area constrain the time of vein formation to Cretaceous-aged compression. Thus the formation of transport-parallel and N65E veins occurred prior to or during motion along the Absaroka thrust fault. Confounding this conclusion is that the areas studied by Mitra et al. (1984) lies about 55 km to the south-west of our study area. Cleavage need not have developed synchronously in both areas.

2.6. Vein strain analysis

All vein types contain twinned calcite grains. This suggests that the veins formed before or during tectonism. Calcite strain data were collected to eliminate the possibility that vein deformation was associated with Basin and Range-aged extension which post-dates thrusting. If vein deformation is related to Basin and Range tectonics, one would expect the maximum shortening direction to be sub-vertical. By contrast, if vein deformation is associated with Cretaceous-aged compression as suggested by the cross-cutting relationships with solution cleavage surfaces, the orientation of the maximum compressional axis should be parallel to the transport direction, although plunges may vary (Spang and Groshong, 1981; Kilsdonk and Wiltschko, 1988).

The calcite strain gauge technique of Groshong (1972, 1974) was applied to two samples using thin sections cut parallel and perpendicular to bedding (data are in Table 1). More than 25 twin sets from the host and vein were measured per thin section to determine the orientation of the principal strain axes (Groshong et al., 1984). Twenty percent of the largest deviations were removed to "clean" the data following the studies of Groshong (1974), Teufel (1980), and Groshong et al. (1984). All samples showed less than a 40% negative expected shear strain values, suggesting that the Twin Creek was not subjected to multiple non-coaxial events (Teufel, 1980). No significant differences in strain magnitude or axis orientations were observed between each vein type or the host. The trend and plunge (273, 22) of the mean maximum calcite twin compressional axis (Fig. 12) is consistent with the typical in-transport bedding parallel shortening observed to the east in the Prospect and Darby thrust sheets of the Idaho–Wyoming fold and

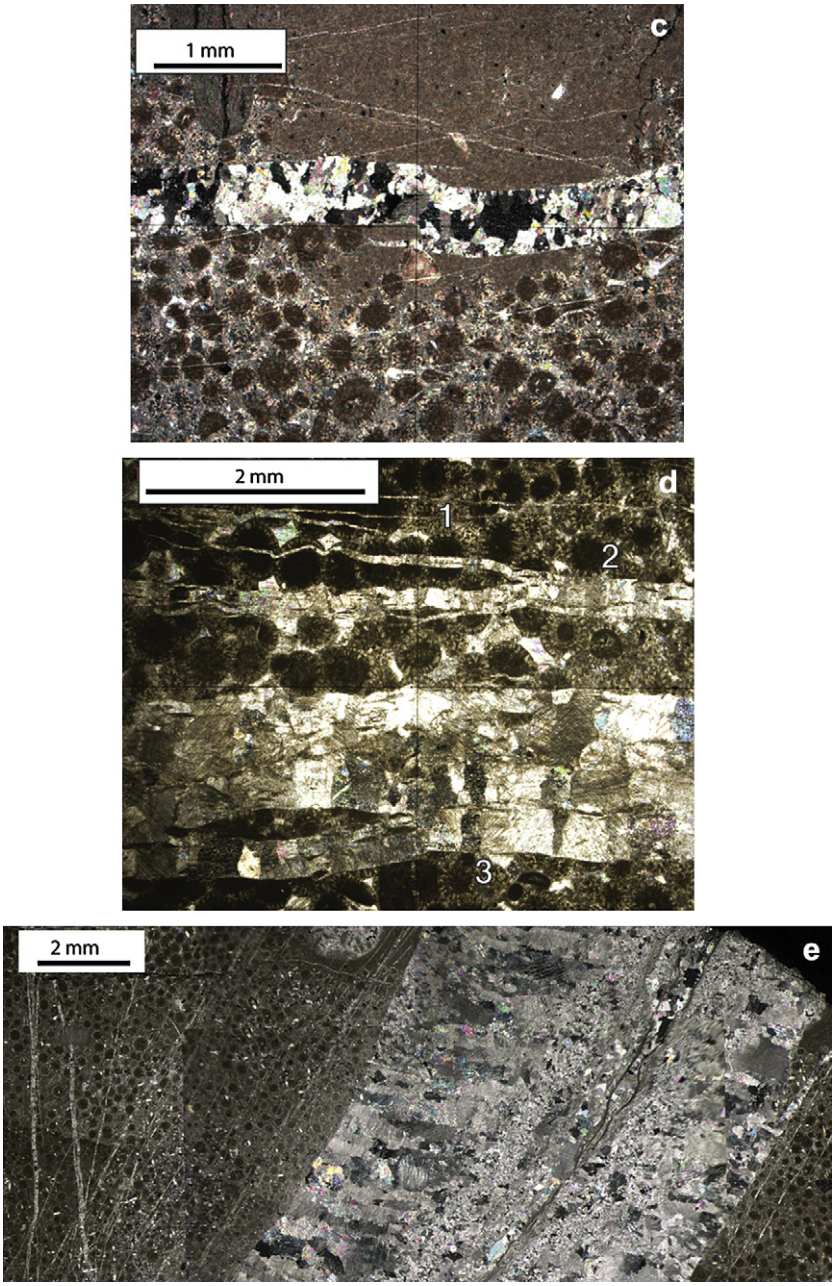

Fig. 11. (*continued*).

thrust belt (Craddock and Wiltschko, 1983) and to the west in the Absaroka thrust sheet proper (Budai and Wiltschko, 1987). The mean maximum compression direction is consistent with east-west tectonic shortening rather than Basin and Range faulting; veining in the Twin Creek limestones was pre- or syn-thrusting.

The transport-parallel veins are most likely syntectonic Mode I cracks formed during a Cretaceous-aged compression event. This interpretation is based on the following: (1) cross-cutting relationships constrain vein formation to the Cretaceous, (2) the orientation of maximum compressional axes are consistent with the formation of transport-parallel Mode I cracks, and (3) timing of cleavage with respect to veining 55 km to the west (Mitra et al., 1984). Nevertheless, we cannot rule out the possibility that veining occurred during motion on the Darby instead of the Absaroka thrust. Until these veins can be more definitively dated, this question will remain somewhat open.

3. Fluid inclusions

Fluid inclusions from 14 oriented calcite vein-bearing samples were examined in doubly polished thick sections using a modified U.S. Geological Survey-type heating-freezing stage manufactured by Fluid-Inc. Due to the small number of measurable inclusions in all samples, several precautions were taken to ensure data precision. First, heating runs were conducted before freezing runs to reduce the possibility of stretching any fluid inclusions during freezing (Prezbindowski and Larese, 1987; Meunier, 1989; Lacazette, 1990). Second, all measurements were made with a blind over the thermocouple readout to remove observational bias. Micro thermometric results were reproducible to within ± 1 °C.

All samples contained small (less than 4 μm), two-phase (liquid and vapor) inclusions. The liquid phase composed 85% to 95% of the total inclusion volume at room temperature. No single-phase

Table 1
Twin Creek calcite mechanical twin data.

Grain type	Optic axis		Twin set		# Twins	Grain widths (μm)	
	IV	Plunge	IV	Plunge		Normal	Parallel
Simple RL2201							
VEIN	181	34E	240	30S	28	720	800
VEIN	135	0	59	23N	28	328	608
VEIN	205	0	136	4.5S	54	480	440
HOST	137	0	46	22N	26	369	240
HOST	78	24E	347	47N	90	800	800
[a]	78	24E	333	2S	3	800	800
HOST	306	33W	7	52N	15	800	800
HOST	90	0	186	24S	20	800	744
Sample RL401							
VEIN	163	18W	51	3.5S	5	448	272
VEIN	83	17W	195	4N	4	800	800
VEIN	214	28E	155	22N	13	600	704
VEIN	34	28W	323	9S	9	520	560
VEIN	8	20E	260	0	3	800	560
VEIN	347	4W	50	5N	10	360	336
VEIN	345	25E	282	37N	8	336	336
[a]	345	25E	226	29N	7	360	296
VEIN	359	4E	290	14N	8	344	248
[a]	359	4E	244	14N	4	280	520
VEIN	115	35E	54	27N	6	176	248
VEIN	232	10W	154	13N	6	296	280
VEIN	151	1W	47	21N	8	480	400
VEIN	6	5E	300	15N	10	520	360
[a]	6	5E	251	15N	7	480	320
VEIN	115	37E	189	15S	12	800	800
VEIN	319	25W	29	10N	10	600	680
VEIN	267	32E	183	7N	23	400	360
VEIN	267	32E	150	49N	8	456	560
VEIN	192	19W	265	3S	8	272	160
VEIN	256	2W	195	0	3	152	184
[a]	256	2W	173	23S	4	184	160
VEIN	64	34W	313	16S	25	504	480
VEIN	187	3W	94	29S	8	272	256
VEIN	221	42W	335	25N	10	680	664
VEIN	129	5E	200	23S	14	400	360
VEIN	221	40W	130	14S	12	280	168
VEIN	5	20E	294	40N	12	416	380
VEIN	262	4E	181	15S	4	368	280
VEIN	146	10E	223	34S	17	800	480
[a]	146	10E	258	5S	5	720	560
HOST	201	56E	152	48N	5	320	560
Sample RL402							
VEIN	72	24W	149	4N	16	280	240
VEIN	196	21E	297	3N	5	560	800
VEIN	110	29E	41	19N	60	800	800
VEIN	288	18W	349	16N	5	224	200
VEIN	206	14E	277	5N	23	336	320
VEIN	220	27E	299	5S	22	360	152
VEIN	213	14E	107	4S	28	800	400
HOST	136	27E	69	7N	10	240	240
HOST	138	20W	249	30N	5	624	520
HOST	201	26E	276	8S	6	96	224
HOST	76	16W	176	4S	1	240	224
HOST	130	29E	229	9S	7	360	320
HOST	262	13W	145	12S	13	432	320
VEIN	73	25W	150	5N	17	280	240
VEIN	110	29E	41	19N	60	800	800
VEIN	286	20W	348	18N	6	200	224
HOST	138	20W	249	30N	5	600	480
VEIN	43	3W	286	2S	22	800	650
VEIN	155	37W	249	11N	12	496	800
VEIN	299	50W	246	48S	50	800	800
VEIN	253	21W	190	13S	7	384	288
VEIN	118	20E	230	8S	50	640	640
VEIN	54	22W	352	20S	20	800	800
[a]	54	22W	309	2N	20	800	800
VEIN	134	5E	70	8N	46	744	368

[a] Denotes second twin set in same grain.

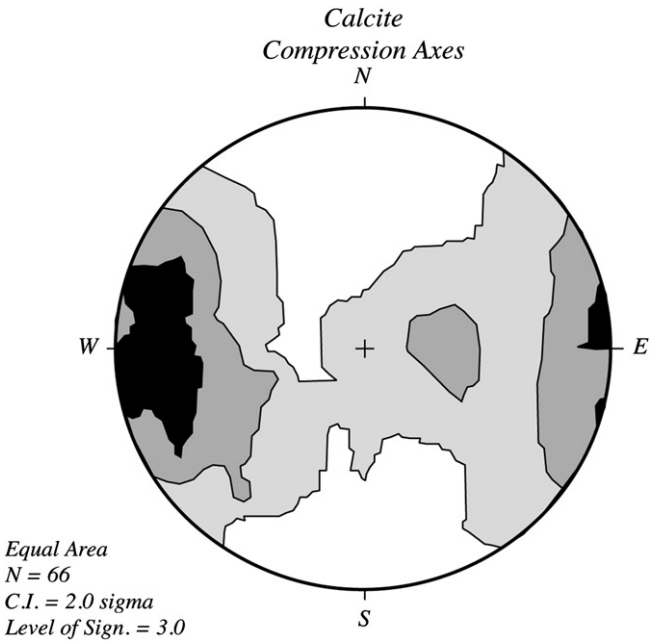

Fig. 12. Lower hemisphere plot of compressional axes contoured according to the method of Kamb (1959). Plotted data include values for both the host and veins. The largest concentration of compressional axes is indicated by the darker shading. Great circle is bedding.

inclusions were observed in any of the vein samples. Daughter minerals such as halite or sylvite were not observed. Due to the cloudy nature of the calcite and small inclusion size, only a few inclusions were suitable for micro thermometric measurements. No measurable inclusions were observed in any of the N40W veins sampled.

All measured inclusions are interpreted as primary inclusions and, therefore, the fluid was originally trapped during vein formation. The evidence for this interpretation includes: (1) the inclusions were not located in trails cross cutting crystal boundaries; and (2) the paired homogenization temperature (T_h) and melting temperature (T_m) values from transport-parallel and N65E vein inclusions produce one cluster (Fig. 13).

3.1. Fluid inclusion results

Freezing was marked by the sudden collapse of the vapor bubble. Although inclusions were cooled to a temperature of −160 °C, all inclusions exhibited complete freezing at temperatures of −50 °C. First melting temperatures (T_{fm}) from all inclusions ranged from −30 °C to −20 °C. This range in T_{fm} approximately corresponds to the eutectic temperature at which liquids first exist with other solids such as ice or hydrous salts in an H_2O–NaCl system during melting. With continued heating the next phase transition was the ice melting at a mean $T_m = -7.0$ °C (Fig. 13). No evidence of clathrate formation was ever observed indicating that little or no CO_2 or CH_4 is present in these inclusions. All available evidence, therefore, indicates that these fluid inclusions are dominated by H_2O + salt (e.g., NaCl). Due to the small size (<4.0 μm) and poor optics related to the turbidness of the twinned calcite precise measurements of the T_m were difficult to obtain. Therefore, the average equivalent wt.% NaCl of 10.5 is based on the average T_m. Homogenization was marked by the disappearance of the vapor bubble at temperatures ranging from 124 °C to 140 °C (Fig. 13). The fluid inclusion data are given in Table 2.

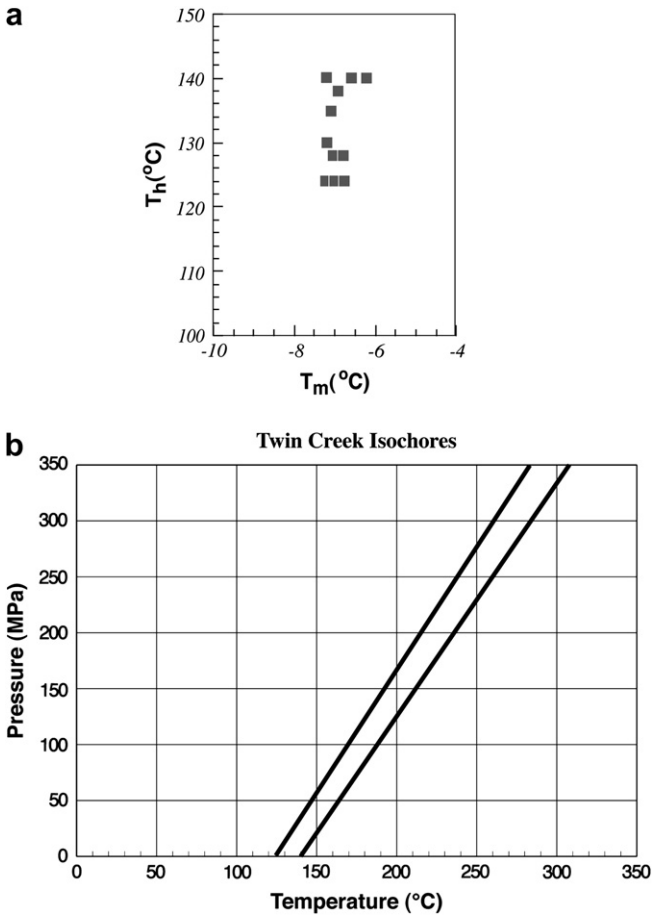

Fig. 13. (a) Scatter plot of all measured homogenization (T_h) and melting temperature (T_m) pairs. (b) *P–T* diagram used to calculate inclusion entrapment temperatures. Isochores calculated using the Brown and Lamb (1989) equation of state.

3.2. Trapping conditions

FLINCOR (Brown, 1989) was used to analyze the measured fluid inclusion data from the Twin Creek syntectonic veins and construct isochores (Fig. 13). The equation of state for the H_2O–NaCl system used in this study is from Brown and Lamb (1989). Although values of T_{fm} are consistent with NaCl, it is difficult to rule out the presence of other salts such as KCl or $CaCl_2$. However, for the combined values of T_m and T_h measured in this study the *P–T* location of the isochores, as shown on Fig. 13, is relatively insensitive to the actual identity of the dissolved salt in the inclusion such that substitution of KCl or $CaCl_2$ for NaCl when determining the *P–T* position of these isochores will not effect the conclusions of this study (Zhang and Frantz, 1987). Values used to construct isochores were the minimum and maximum T_h of 124 °C and 140 °C, respectively, and the mean $T_m = -7$ °C. These isochores bound the range of temperatures and pressures that are consistent the compositions and molar volumes of the fluids contained in the fluid inclusions (Fig. 13).

Table 2
Twin Creek limestone vein fluid inclusion data.

Sample #	T_{fm} (°C)	T_m (°C)	T_h (°C)	Size (μm)	Notes
RL801					
1	−35	−6.6	140	5.4 × 2.7	
2	−22	−6.9	139	5.4 × 2.7	
3	−26	−7.0	124	8.1 × 4.0	
4	−23	−6.2	?	?	Leaked
5	−30	−7.1	?	?	Leaked
RL401					
1	?	?	140	1.4 × 1.4	
RL1701					
1	−25	−6.8	124	1.8 × 2.7	
2	−30	−7.2	124	1.9 × 2.7	
3	−29	?	?	2.7 × 2.7	Small
RL901					
1	?	−7.2	140	1.8 × 1.8	Small
RL1201					
1	−28	−6.8	128	2.7 × 2.7	
2	−26	−7.1	135	2.7 × 4.0	
RL1801					
1	−26	?	?	2.7 × 8.1	Poor
2	−22	−7.2	130	5.4 × 3.4	
RL2701					
1	?	?	138	2.7 × 2.7	

4. Stable isotopes

The compositions of syntectonic veins have been studied by a variety of means to understand the fluid source, composition, and temperature (e.g. Rye and Bradbury, 1988; Erel and Katz, 1990; Bottomley and Veizer, 1992; Shemesh et al., 1992; Hilgers and Sindern, 2005; Cervantes et al., 2004; Hilgers et al., 2006). These studies have shown that small-scale cross and longitudinal variations in trace metals and stable isotopes of both oxygen and carbon may be preserved. The veins may preserve calcite which precipitated from fluids that are significantly different from the local host (Rye and Bradbury, 1988; Erel and Katz, 1990); the fluid sources for veins of different generations may also be determined (Gao et al., 1992; Shemesh et al., 1992). Since the temperature dependence of oxygen isotope fractionation in a calcite–water system is well studied (Epstein et al., 1953; Craig, 1965; Friedman and O'Neil, 1977), if constraints can be placed on the composition of the vein fluid, a temperature of vein precipitation may be derived.

Samples of vein and host carbonate were removed from a large number of oriented billets with the aid of a microscope mounted drill. Samples were collected in a traverse perpendicular to the host/vein interface. The sampled carbonate was reacted with phosphoric acid at 75 °C producing CO_2 gas. The resulting gas was analyzed for carbon and oxygen isotope ratios on a Finnigan MAT 251 mass spectrometer. Isotope ratios were measured relative to NBS-20 and are reported relative to PDB. Results are reproducible to ±0.14‰ for $\delta^{13}C$ and ±0.25‰ for $\delta^{18}O$. The results are displayed in Fig. 14.

The mean carbon isotope values for vein and host are 2.10 and 1.66, respectively. The standard deviation for both are 0.50 and 0.42, respectively. Likewise, the oxygen isotopic means for vein and host are −10.01 and −11.04 with standard deviations of 1.04 and 0.39, respectively. The mean oxygen values for both vein and host are significantly lighter than the global marine Jurassic value of about 2.0 (Prokoph et al., 2008). The limited data in Sorkhabi (2005) show that nearly all units above the Triassic have been reset to lighter oxygen values than global means.

A parametric ANOVA (analysis of variance) shows that to the 95% confidence interval the vein and host oxygen and carbon population means for both carbon and oxygen are significantly different. Because the populations are not normally distributed (see Table 3), a non-parametric test was also performed on the ranked oxygen and carbon values. These tests also indicate to the same level of confidence that oxygen and carbon populations for both veins and host determinations are different.

The isotopic zonation in individual transport-parallel or N65E veins is very small (Fig. 15). This is consistent with the CL and PPL results, suggesting that fluid with a nearly constant fluid composition was the source for both the transport-parallel and N65E veins. Moreover, the mean vein and host isotopic compositions are within 1‰ of each other, suggesting that the vein fluid and the host

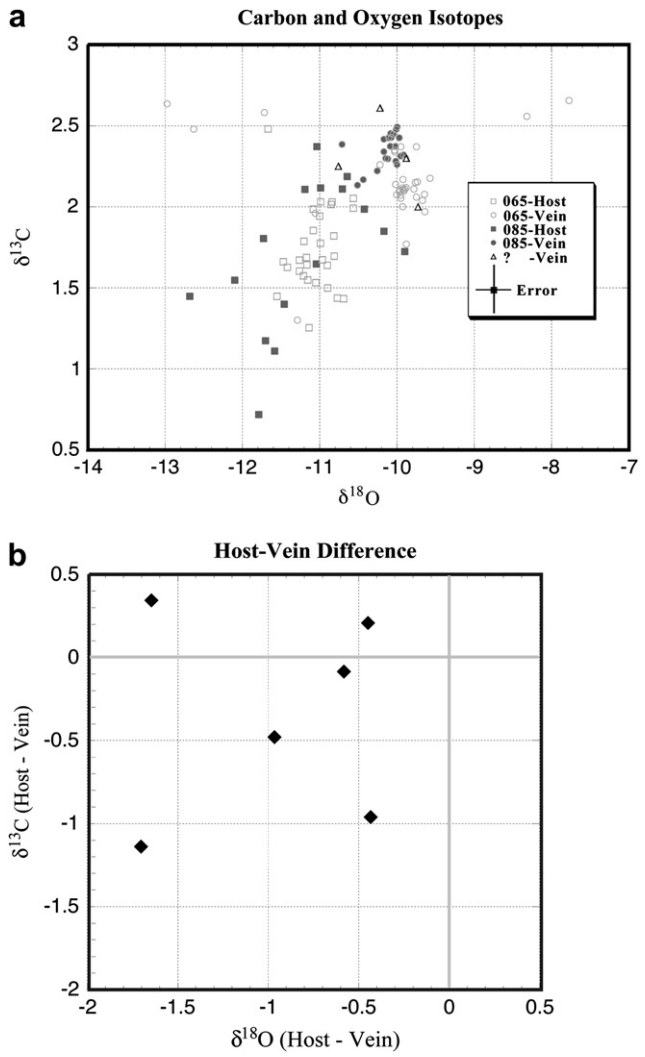

Fig. 14. (a) Carbon and oxygen isotopic composition of the Twin Creek Limestone. (b) Difference between host and vein carbon and oxygen isotopic values.

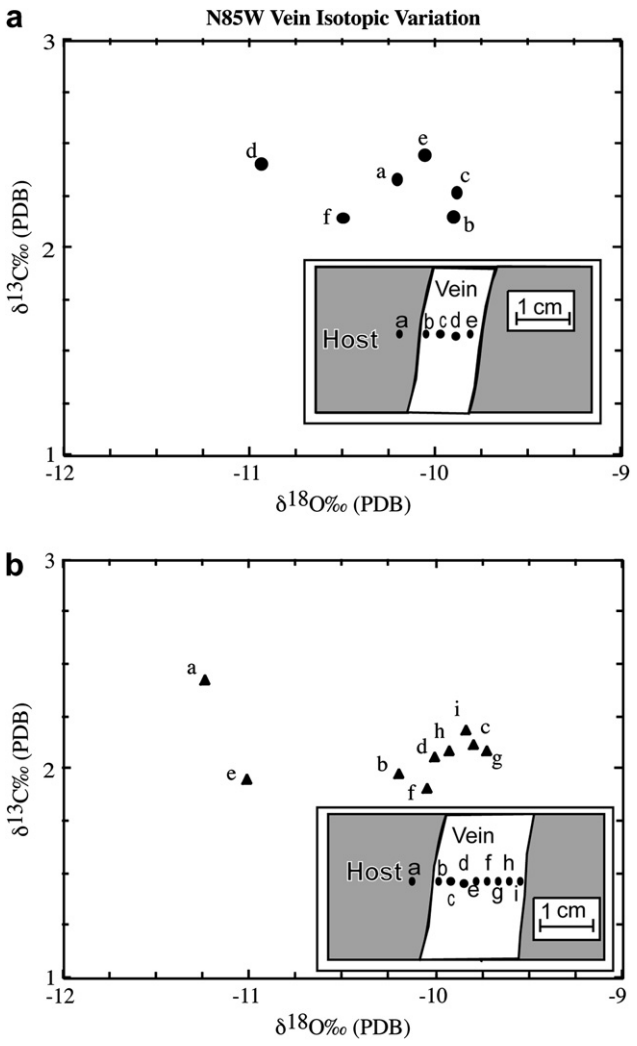

Fig. 15. Carbon and oxygen isotope variation within individual vein types. (a) N85W veins (sample 502). (b) N65E veins (sample 1801). Inset figure shows the traverse method of sampling.

were nearly in isotopic equilibrium even though a statistically significant offset exists (Fig. 14).

Estimates of vein fluid temperatures can only be achieved if constraints can be placed on the fluid's isotopic composition. The similarities between the $\delta^{18}O$ and $\delta^{13}C$ compositions of both the host and the veins suggest that (1) the vein fluid was in isotopic equilibrium with the host during vein formation, or (2) the original isotopic compositions of both the veins and the host have been altered to their present values since deposition. Regardless of the method, the Twin Creek veins are equilibrated with the host and constraining the original $\delta^{18}O$ composition of the fluid is not possible. Thus attempts to utilize the temperature dependence of oxygen isotopes as an accurate paleothermometer in this case seem unlikely.

Table 3
Statistical comparison of oxygen and carbon isotope data.

	Oxygen		Carbon	
	Vein	Host	Vein	Host
Mean	−10.01	−11.04	2.10	1.66
Standard deviation	1.02	0.62	0.50	0.42
Minimum	−13.41	−13.04	−1.79	0.15
Maximum	−5.09	−9.90	2.83	2.48
Skewness	−0.49	−1.13	−4.57	−1.44
Kurtosis	6.91	2.19	30.93	3.61

Because the host and veins have nearly the same isotopic signature, one of the two following fluid flow systems must be responsible for this equilibrium condition.

4.1. Closed system

The Twin Creek may have been closed to outside fluid flow during vein formation. If so, the pore fluid and the rock (host) were in equilibrium before and during vein formation. Given that there is more rock than water, the isotopic composition of the rock would control the fluid composition, especially for carbon isotopes. The evidence for closed system conditions in the Twin Creek is that, statistically, the host and vein isotopic values are the same. In addition, the carbon isotopic values from Jurassic carbonates worldwide and those of the Twin Creek host and veins are the same (Prokoph et al., 2008).

In a closed system the temperature of the host and the vein fluid are equal. Therefore, the temperatures computed for vein formation using fluid inclusions must apply to the host as well. Since the minimum temperature (178 °C using the 25 °C/km gradient) is larger than that predicted from 2.75 km of overburden (74 °C),

erosion did not keep up with the vertical component of thrust motion.

4.2. Open system

The host may have been altered by an outside fluid source (Burtner and Nigrini, 1994). Many variations of this open system may have occurred. For example, the whole system (host and vein) may have been altered to their present value by an imported fluid. Alternatively, an outside fluid from which the veins were precipitated may have filled the fractures only after the host and this fluid reached equilibrium. Both alternatives require wholesale alteration of the host rock. While there is no petrographic evidence for such a wholesale resetting, the oxygen isotopic values we measure for both the host and veins are lighter by at least 8 ‰ than global values reported by Prokoph et al. (2008). Because both host and veins are lighter, we conclude that the resetting took place before vein formation.

We conclude that a relatively closed system prevailed. The isotope results indicate that whatever temperature constraints we derive for the host also apply to the veins. This is because the similarity in vein and host isotopic composition suggests the fluid from which the vein precipitated was close to thermal equilibrium with the host.

5. Discussion

Although we do not know the point along some, perhaps complex, time–temperature path at which the veins studied were filled, there are constraints on the thermal evolution of the region. Burtner and Nigrini (1994) used apatite fission track and vitrinite reflectance data from the Gulf 1 Huff Lake Federal well (Fig. 1) to construct a time-temperature model for two Cretaceous sandstone units overlying the Jurassic Twin Creek Limestone (Fig. 16). A period of relatively high temperature from 100 to 90 Ma was required to match the high vitrinite reflectance values at shallow depths and low vitrinite reflectance gradient in the well. Burtner et al. (1994) based on more data found that the geothermal gradient for the period before 90 Ma was probably lower, although no value was given. The cooling event from 90 to 80 Ma is interpreted as due to disruption of out-of-the-basin flow of hot fluid by motion on the Crawford–Meade thrust and subsequent cooling.

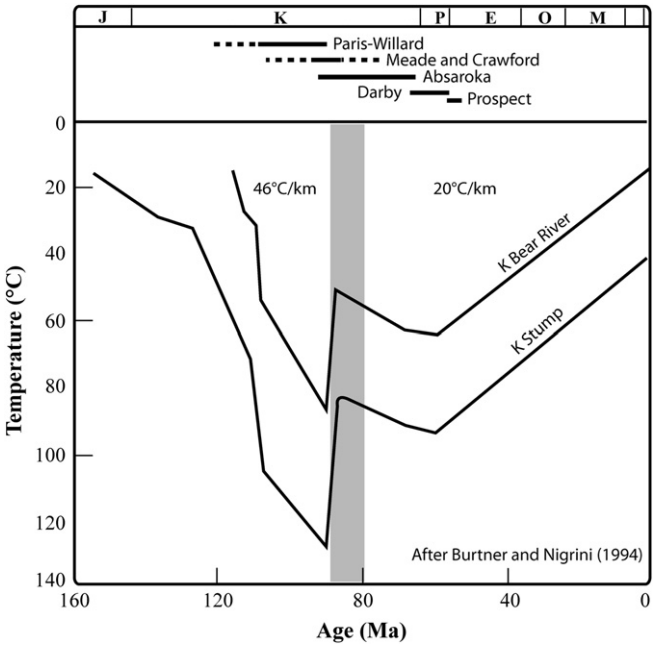

Fig. 16. Sketch illustrating one time-temperature path the Twin Creek Formation may have been subject to since deposition. The position occupied during veining along this hypothetical or any other path related to this study is unknown. After Burtner and Nigrini (1994), Fig. 11. The thermal history was constructed from modeled apatite fission track ages and vitrinite reflectance values from the Gulf 1 Huff Lake Federal well; see Fig. 1 for location. Thrust timing data from Wiltschko and Dorr (1983).

The well studied by Burtner and Nigrini (1994) penetrates the Crawford–Meade thrust plate and lies about 50 km to the south of our study area. In addition, the units studied are sandstone that can reasonably expected to be more efficient hydrologic flow units compared to the Jurassic Twin Creek Limestone. Nevertheless, if the same pattern found by Burtner and Nigrini (1994) repeats for the Absaroka and Darby thrust sheets, one would expect heating above what one would expect from simple burial followed by sudden cooling as motion on the Absaroka thrust fault took place. A similar study in the footwall of the Absaroka thrust sheet would be required to confirm this pattern.

In the following, we assume that during vein precipitation the temperature and pressure were near peak. We start our discussion of the constraints on fluid pressure by, first, assuming a 25 °C/km geothermal gradient and then plotting the thermobaric gradients for (1) lithostatic (26 MPa/km) and (2) hydrostatic (10 MPa/km) pressure, and (3) the isochores derived from fluid inclusions. We examine higher geothermal gradients and limitations below. Fluid pressure associated with vein formation must have been less than or equal to lithostatic because fluid pressures in excess of lithostatic presumably cannot be maintained in the crust for extended periods of time (although see Roedder, 1984). The minimum fluid pressure must be equal to or greater than normal hydrostatic pressure at whatever depth the vein minerals precipitated. It is clear that under the 25 °C/km assumption, that the fluid pressure may lie anywhere between 50 MPa and 300 MPa (Fig. 17a).

One way to limit this range of trapping pressures is to have independent data on the trapping temperatures or pressures from depth of burial estimates assuming conduction is the only heat transport mechanism. Although the actual amount of overburden during vein formation is unknown, constraints may be placed on the maximum and minimum depth of burial (Fig. 17a) using geologic map data from the surrounding area (Rubey, 1973). The minimum amount of overburden was most likely 2.75 km. The expected temperature at this depth would be 74 °C, still assuming a 25 °C/km geothermal gradient. The pressure would lie between a hydrostatic pressure of 27.5 MPa (point A, Fig. 17a) and a lithostatic pressure of 71 MPa (point B, Fig. 17a). These points do not lie on the isochores. Alternatively, the maximum amount of overburden could have been 7.75 km, if no erosion occurred during thrusting (Fig. 17a, inset). The temperature expected for this depth is 200 °C. The pressure at this greater depth could range between hydrostatic (point C, 77.5 MPa, Fig. 17a) and lithostatic (point D, 201 MPa, Fig. 17a). The lower-bound isochore calculated from fluid inclusions is closest to the hydrostatic pressure (point C). Remember, though, that the 7.75 km depth of burial is an extreme value. Accepting this value requires the instantaneous emplacement and thermal equilibration of the entire Absaroka hanging wall above the study area.

Without further constraints, it appears that one must conclude that a hydrostatic fluid pressure most likely existed in the veins during thrusting. Nevertheless, we next explore alternatives to the assumptions we have made leading to this conclusion.

5.1. Thrust faulting and overburden temperatures

Geologic evidence south of our area in the Idaho–Wyoming fold and thrust belt (Fig. 1) shows that thick sequences of Cretaceous and lower Tertiary clastics were being eroded from hanging walls during thrust belt motion (Royse et al., 1975). Warner and Royse

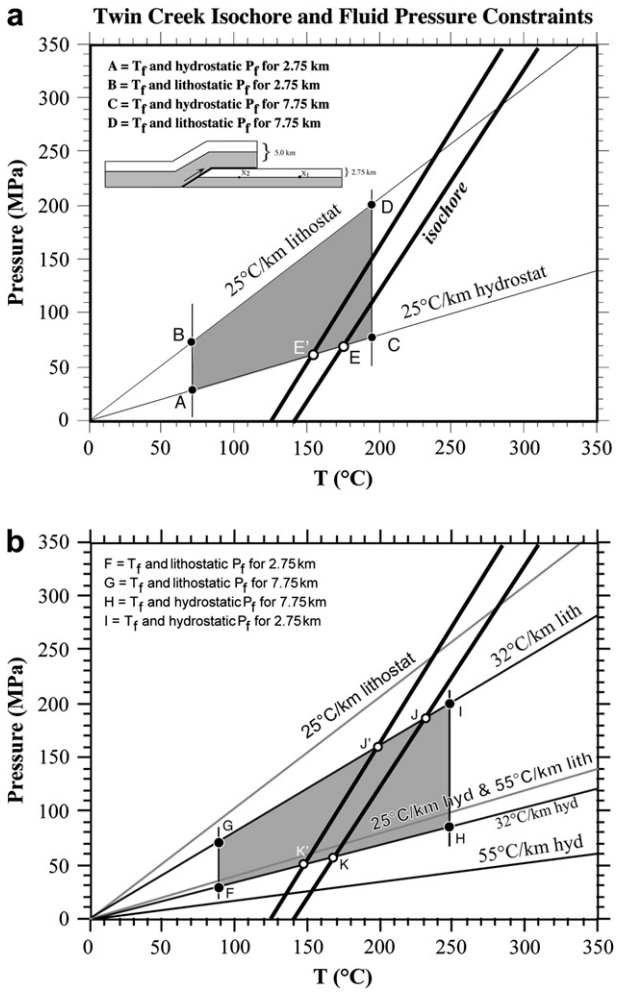

Fig. 17. *P–T* diagram used to constrain inclusion entrapment temperatures. The shaded regions indicate constrained pressure and temperature ranges. The labeled points are discussed in the text. Thick lines are isochores from Fig. 13. Present total stratigraphic thicknesses (eroded and uneroded) were used for values in the inset. (a) 25 °C/km geothermal gradient. (b) 32 °C/km and 55 °C/km geothermal gradients. Symbols: T_f, fluid temperature; P_f, fluid pressure.

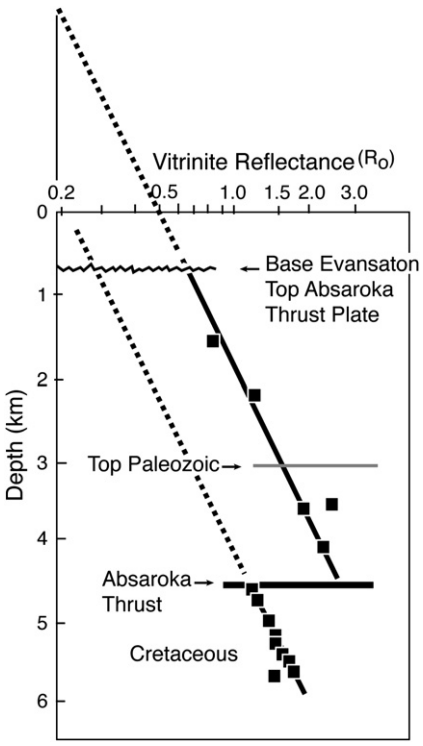

Fig. 18. Vitrinite reflectance versus depth at Whitney Canyon field. Dashed lines show projection of reflectance lines to intersection with 0.2% R_o baseline. More than 3 km (10,000 ft) of section was eroded from the hanging wall after the reflectance slope was established and before the deposition of the Evanston Formation (75–72 Ma) (after Warner and Royse, 1987).

(1987) suggest that the rate of erosion approximately equaled the vertical component of the thrust motion within the Absaroka thrust fault to the south. In their view, the hanging wall did not contribute to the overburden above the footwall; it was eroded as quickly as it was emplaced (see also Burtner et al., 1994). This argument is based on a comparison of thermal gradients computed from vitrinite reflectance (R_o) data and thermal alteration index (TAI) data between both duplicated and non-duplicated stratigraphic sections. The footwall R_o profile projects back to the R_o baseline value of 0.2% (Dow, 1977) near the present ground surface (Fig. 18). This result means that the footwall was never buried to a depth greater than the amount that exists now for any significant period of time. This idea is also supported by the offset of the reflectance profiles at the Absaroka thrust (Fig. 18). This offset indicates that the top of the footwall was never buried as deeply as the bottom of the hanging wall. Warner and Royse (1987) also suggest that the apparent parallelism and offset between the hanging wall and footwall reflectance profiles indicate that no large perturbation of the geothermal gradient has occurred in this area. Similar results are obtained by them from the Darby thrust and other parts of the Wyoming fold and thrust belt. This suggestion is counter to model predictions where no erosion is assumed (e.g., Oxburgh and Turcotte, 1974; Smith and Wiltschko, 1996).

Assuming that similar conditions existed 50–80 km to the north of our study area, the amount of overburden above the Twin Creek Formation would have remained close to the minimum of 2.75 km. Referring to Fig. 17a, if 2.75 km is the more reasonable value for overburden, then our starting assumption of a 25 °C/km geothermal gradient must be incorrect for the fluid inclusion data to be honored.

5.2. Geothermal gradient constraint

What geothermal gradient would be required to both honor the fluid inclusion data and produce lithostatic fluid pressures? As shown above, if one assumes a geothermal gradient of 25 °C/km, the trapping fluid pressures and temperatures must lie between points A, B, C and D in Fig. 17a. Thus, the fluid pressure during vein formation was only slightly higher than the expected hydrostatic value for a 7.75 km depth of burial (Fig. 17a). Reducing the maximum depth of burial moves the maximum fluid pressure toward the hydrostat along the isochore. The intersections of the isochores with the 25 °C/km hydrostat (points E, E′, Fig. 17a) represent the minimum amount of overburden that may have existed in keeping with the fluid inclusion data during vein formation (equivalent to 5.5–7.2 km). If this value represented the actual overburden, the fluid pressure would be nearly hydrostatic (55–72 MPa).

Increasing the temperature of the fluid would increase the fluid pressure along the isochores. Assuming a 32 °C/km geothermal gradient, the fluid pressures and temperatures that could be present during vein formation would be within a quadrilateral in pressure-temperature space whose apices are F, G, H and I (Fig. 17b). In the unlikely event that a great portion of the hanging-wall stratigraphy covered the field location during veining, fluid pressures equal to lithostatic could be achieved (points J, J′). Alternatively, the intersection of the 32 °C/km hydrostatic gradient

and the isochore (point J, Fig. 17b) represents a minimum amount of overburden of 4.9–5.4 km.

Producing a fluid pressure equal to lithostatic pressure requires a geothermal gradient in excess of 32 °C/km with little erosion during thrusting. Increasing the geothermal gradient would produce lithostatic fluid pressures with less overburden (see 55 °C/km geotherm, Fig. 17b).

We conclude that the fluid pressure during vein formation in the footwall of the Absaroka may have been near hydrostatic for all overburden estimates. We have assumed that the fluid temperature is not higher than the ambient host—an assumption that is supported by isotope data.

Hydrostatic fluid pressure within the veins of the Twin Creek Formation presents the mechanical difficulty of explaining the existence of the precursory cracks. If elevated fluid pressure, at least in relation to the least (vein normal) principal stress, is required for Mode I cracking, then why is this fluid pressure not preserved in the fluid inclusions?

5.3. Fluid inclusion assumptions

We have assumed that the molar volumes of the fluids trapped in the inclusions reflect the *P–T* conditions of vein formation. As discussed previously, certain fluid inclusion characteristics (e.g., textures) are consistent with fluid trapping during vein formation. However, these characteristics do not preclude the possibility that although the fluid inclusions were originally formed when the vein minerals grew, these inclusions were modified at some time after vein formation. Of particular concern for the inclusions in calcite is that certain changes in *P–T* can yield increases in the volume of fluid inclusions, a process known as stretching (e.g., Roedder, 1984; Prezbindowski and Larese, 1987). These changes in fluid inclusion volumes are driven by differences between the lithostatic pressure exerted on the grain that contains the fluid inclusion (the external pressure or P_{ext}) and the pressure within the fluid inclusion (the internal pressure or P_{int}). Typically, conditions of $P_{int} > P_{ext}$—conditions that may result in stretching—are produced by an increase in *T* and/or a decrease in *P*. For example, the fluid inclusions in this study have molar volumes consistent with *P–T* conditions that fall along the isochores shown in Fig. 13. If these inclusions were subjected to *P–T* conditions on the high temperature side of these isochores, P_{int} would become greater than P_{ext}. If the difference between P_{int} and P_{ext} is sufficiently large, the inclusion will undergo stretching and, therefore, the molar volume will decrease effectively shifting the isochores to higher temperature, lower pressure conditions. Thus, stretching will result in an increase in the values of the homogenization temperature. In the following paragraphs we explore the implications of inclusion formation followed by stretching for the Twin Creek veins.

As shown in Fig. 13, homogenization temperatures range from 124 °C to 140 °C. Whether these temperature reflect vein formation, or later stretching they represent the minimum temperature that these veins experienced. These temperatures are consistent with the highest temperatures recorded along the time-temperature path shown on Fig. 16 and suggest that the veins were in place during or prior to the 90–100 Ma period of maximum temperatures. If these inclusion were formed and then were modified by stretching, this implies vein formation occurred sometime prior to this 90–100 Ma period of maximum temperatures.

If the fluid inclusions did not undergo modification, the relatively high-temperature/low-pressure location of the isochores indicate that fluid pressures were less than lithostatic pressure during vein formation. Alternatively, fluid pressures may have been lithostatic during vein formation, but the molar volume of the fluids in the fluid inclusions would not reflect these conditions if they had undergone stretching after vein formation. For example, at 26 MPa/km the lithostatic pressure would fall between approximately 70 and 200 MPa based on our overburden estimates. At 25 °C/km this would require fluid inclusion trapping temperatures of approximately 70–195 °C (Fig. 17). The fluid inclusion isochores do not intersect these *P–T* conditions (Fig. 17). However, modification of inclusion via stretching can reconcile this apparent discrepancy. Intersection of our measured isochores with a lithostatic pressure and temperature curve would require a post-entrapment temperature increase, pressure decrease, or some combination of the two in order to intersect the isochores based on the molar volume of fluids now in the inclusions (Fig 17).

5.4. Fracture propagation

Another ready explanation for the apparent low fluid pressure during vein formation is that the elevated fluid pressure event was brief in relation to the time required to precipitate calcite. For a fracture to form, the fluid pressure inside the crack must exceed both the normal stress on the fracture wall and the resistance of the rock to cracking, i.e., fracture toughness, for Mode I cracking (e.g., Atkinson, 1984). The existence of filled fractures in this outcrop indicates that a significant driving stress existed for these fractures to form. This implies that the fluid pressure was not hydrostatic over the long-term but instead was sufficiently high to cause fracture to propagation. The total width-to-length ratios of the veins and presumed elastic properties seem to indicate the need for a high driving stress. However, we see no evidence of large open fractures into which euhedral calcite grew. If instead the veins grew incrementally through the addition of small fractures as indicated by the thin host inclusions in some veins, then the required driving stress is less. The fact that the veins studied largely occur in vein arrays provides a mechanism to further reduce the required driving stress. This would be especially the case where crack tips overlap the midsections of other array members, which the case in our vein arrays (e.g., array B, Fig. 7).

The parameters that can change the local driving stress include (1) increase in joint volume and therefore drop in fluid pressure during fracture propagation and (2) flow of fluid from the permeable host into the crack or the previously formed crack body into the newly created portion of the crack tip. If we then consider the fluid to be aqueous, it is possible to compute the fluid pressure drop due to an increment of crack propagation. Compressibility (isothermal) is defined as

$$\beta_w = \frac{1}{K_w} = \frac{-1}{V_w}\left(\frac{\partial V_w}{\partial P_f}\right)_{(T,M)} \tag{4}$$

where β_w is the fluid compressibility (units $1/P$), K_w is the bulk modulus of fluid, V_w the bulk fluid volume. For a small isothermal increment of volume change,

$$dP_f = -\frac{dV_w}{\beta_w V_w} \tag{5}$$

The compressibility of water is a function of temperature and pressure but it is on the order of 4.0×10^{-11} cm^2/dyne. If the volume of a vein increases by 1%, the pressure drop is 25 MPa. There is no evidence of a gas in these fractures from either the isotopes or fluid inclusions; Lacazette and Engelder (1992) showed that methane in a fracture can have a profound effect on the pressure conditions inside a propagating fracture.

This drop in pressure is mitigated by fluid flow into the newly formed crack increment. Re-establishing the pressure in the crack is both a function of the permeability of the host, the pressure

gradient from the host to the crack, and flow from the pre-existing crack body into the newly formed crack propagation increment. Therefore, if fracture propagation is more rapid than fluid flow into the crack, then one would expect the fluid within the crack to have a pressure less than the background pressure in the bulk porous host. If the vein calcite precipitated at this time, then the pressure recorded by the fluid inclusions, even if unmodified by later stretching, would be less than the ambient remote fluid pressure.

One can therefore envision a scenario where a pulse of elevated driving stress (local increase in fluid pressure or decrease in fracture-normal stress) causes cracking at a particular location. The first or small group of array crack members propagates from local stress concentrations, relieving the vein-normal stress locally. Diffusion from the host from the host into the crack initiates precipitation. The fluid pressure stays low until flow re-establishes the fluid pressure to pre-cracking values. Diffusion and flow from the adjacent host into the crack of saturated fluid in isotopic equilibrium initiates precipitation, especially if the partial pressure of CO_2 is also low, reducing the solubility of calcite in the fracture (see Morse and Mackenzie, 1990). The veins would grow and fill in cracks closest to the source of fluid, i.e., near the vein walls, in a syntaxial way. After crack propagation, the fluid pressure falls, perhaps to near hydrostatic values. This can only take place if the drop in internal fluid pressure due to crack growth outpaces fluid pressure build-up from the host pore fluid. The low fluid pressure we compute from the fluid inclusions may reflect the trade-off between strength and/or permeability of the Twin Creek Limestone.

6. Conclusions

(1) Isotope data suggest that the pore fluids were in equilibrium with the host at the time of vein deposition and that the fluid flow system was essentially closed to outside sources during vein precipitation.
(2) Analysis of fluid inclusions trapped within syntectonic veins in the footwall of the Absaroka thrust fault suggests that the fluid pressures during vein precipitation may have been near hydrostatic using a reasonable range of geothermal gradients.
(3) Using acceptable geothermal gradients suggests that erosion did not keep up with the vertical component of thrust motion. Thus the Twin Creek must have been buried to a depth greater than 2.75 km during vein formation.
(4) The fluid pressure had to be sufficient to provide a driving stress required for fracture propagation. The low fluid pressure in the veins could record precipitation after propagation but before a higher ambient fluid pressure was re-established.

Acknowledgments

This paper is based on the MSc thesis of RL at Texas A&M University. Thanks to the American Association of Petroleum Geologists and the Colorado Scientific Society for thesis support. We'd also like to thank Ethan Grossman for assistance with collection and interpretation of the isotopic results, Sherry Bame for the isotope statistical analyses and Ray Guillemette for microprobe analyses. Mike Howell assisted in the field. NSF award EAR-9219986 partially supported this project.

References

Anders, M.H., Geissman, J.W., Piety, L.A., Sullivan, J.R., 1989. Parabolic distribution of circum-eastern Snake River Plain seismicity and latest Quaternary faulting: migratory pattern and association with the Yellowstone hotspot. Journal of Geophysical Research 94, 1589–1621.

Armstrong, F.C., Oriel, S.S., 1965. Tectonic development of Idaho–Wyoming thrust belt. American Association of Petroleum Geologists Bulletin 71, 1847–1866.

Atkinson, B.K., 1984. Subcritical crack growth in geological materials. Journal of Geophysical Research 89, 4077–4114.

Beach, A., 1975. The geometry of en echelon vein arrays. Tectonophysics 28, 245–263.

Beach, A., 1977. Vein arrays, hydraulic fractures and pressure-solution structures in a deformed flysch sequence, S.W. England. Tectonophysics 40, 201–225.

Bottomley, D.J., Veizer, J., 1992. The n nature of groundwater-flow in fractured rock—evidence from the isotopic and chemical evolution of recrystallized fracture calcites from the Canadian Precambrian Shield. Geochimica et Cosmochimica Acta 56, 369–388.

Brown, P.E., 1989. FLINCOR: A microcomputer program for the reduction and investigation of fluid-inclusion data. American Mineralogist 74, 1390–1393.

Brown, P.E., Lamb, W.M., 1989. P-V-T properties of fluids in the system H2O±CO2±NaCl: New graphical presentations and implications for fluid inclusion studies. Geochimica et Cosmochimica Acta 53, 1209–1221.

Budai, J.M., D.V. Wiltschko, 1987, Structural controls on syntectonic diagenesis within the Haystack Peak region of the Absaroka thrust sheet, Idaho–Wyoming–Utah Thrust Belt: Wyoming Geological Association Guidebook—38th field conference, pp. 55–68.

Burtner, R.L., Nigrini, A., 1994. Thermochronology of the Idaho-Wyoming thrust belt during the Sevier orogeny: a new, calibrated, multiprocess thermal model. American Association of Petroleum Geologists Bulletin 78, 1568–1612.

Burtner, R.L., Nigrini, A., Donelick, R.A., 1994. Thermochronology of Lower Cretaceous source rocks in the Idaho-Wyoming thrust belt: AAPG Bulletin 78, 1613–1636.

Cervantes, Pablo, Wiltschko, David V., Sharp, Zachary, 2004, Kinematics of vein growth and evolution in the Ouachitas, Arkansas:: Geol. Soc. America Abstr w. Programs, 36, paper 11–12.

Craddock, J.P., Wiltschko, D.V., 1983. Strains in the Prospect thrust sheet, Overthrust belt, Wyoming (abs). Geological Society of America Abstracts with Program 15, 520.

Craig, H., 1965. The measurement of oxygen isotope paleotemperatures. In: Tongiorgi, E. (Ed.), Stable Isotopes in Oceanographic Studies and Paleotemperatures. Consiglio Nazionale delle Richerche, Laboratorio de Geologia Nucleare, Pisa, pp. 161–182.

Dahlen, F.A., Suppe, J., Davis, D., 1984. Mechanics of fold-and-thrust belts and accretionary wedges: cohesive coulomb theory. Journal of Geophysical Research 89 (B12), 10087–10101.

Davis, D., Suppe, J., Dahlen, F.A., 1983. Mechanics of fold and thrust belts and accretionary wedges. Journal of Geophysical Research 88, 1153–1172.

DeCelles, P.G., 1994. Late-Cretaceous-Paleocene synorogenic sedimentation and kinematic history of the Sevier thrust belt, northeast Utah and southwest Wyoming. Geological Society of America Bulletin 106, 32–56.

DeCelles, P.G., Pile, H.T., Coogan, J.C., 1993. Kinematic history of the Meade thrust based on provenance of the Bechler Conglomerate at Red Mountain, Idaho, Sevier thrust belt. Tectonics 12, 1436–1450.

Dixon, J.S., 1982. Regional structural synthesis, Wyoming salient of western overthrust belt. American Association of Petroleum Geologist Bulletin 66, 1560–1580.

Dow, W.G., 1977. Kerogen studies and geological interpretations. Journal of Geochemical Exploration 7, 79–99.

Epstein, S., Buchsbaum, R., Lowestam, H.A., Urey, H.C., 1953. Revised carbonate water isotopic temperature scale. Geological Society of America Bulletin 64, 1315–1326.

Erel, Y., Katz, A., 1990, Trace-element distribution across calcite veins; a tool for genetic interpretation: Chemical Geology, 85, 361–367.

Foreman, J.L., Dunne, W.M., 1991. Conditions of vein formation in the southern Appalachian foreland: constraints from vein geometries and fluid inclusions. Journal of Structural Geology 13 (10), 1173–1183.

Friedman, I., O'Neil, J.R., 1977. Compilation of stable isotope fractionation factors of geochemical interest. In: Data of Geochemistry, sixth ed. U.S. Geological Survey Professional Paper, 440 pp.

Gao, G., Elmore, R.D., Land, L.S., 1992. Geochemical constraints on the origin of calcite veins and associated limestone alteration, Ordovician Viola Group, Arbuckle Mountains, Oklahoma, U.S.A. Chemical Geology 98, 257–269.

Gentry, D.J., 1983. Solution cleavage in the Twin Creek Formation and its relationship to thrust fault motions in the Idaho–Utah–Wyoming thrust belt. M.S. thesis, University of Wyoming, Laramie, 51 pp.

Groshong, R.H., 1972. Strain calculated from twinning in calcite. Geological Society of America Bulletin 83, 2025–2038.

Groshong, R.H., 1974. Experimental test of least- squares strain gage calculation using twinned calcite. Geological Society of America Bulletin 85, 1855–1864.

Groshong, R.H., Teufel, L.W., Gasteiger, C., 1984. Precision and accuracy of the calcite strain-gauge technique. Geological Society of America Bulletin 95, 357–363.

Hilgers, C., Kirschner, D., Breton, J., Urai, J., 2006. Fracture sealing and fluid overpressures in limestones of the Jabal Akhdar dome, Oman mountains. Geofluids 6, 168–184.

Hilgers, C., Sindern, S., 2005. Textural and isotopic evidence on the fluid source and transport mechanism of antitaxial fibrous microstructures from the Alps and the Appalachians. Geofluids 5, 239–250.

Hubbert, M.K., Rubey, W.W., 1959. Role of pore pressure in mechanics of overthrust faulting—I. Mechanics of fluid-filled porous solids and its application to overthrust faulting. Geological Society of America Bulletin 70, 115–166.

Jacobson, S.R., Nichols, D.J., 1982. Palynological dating of syntectonic units in the Utah–Wyoming thrust belt: the Evanston Formation, Echo Canyon Conglomerate, and Little Muddy Creek Conglomerate. In: Powers, R.B. (Ed.), Geologic Studies of the Cordilleran Thrust Belt. Rocky Mountain Association of Geologists, vol. II, pp. 735–750.

Jaeger, J.C., Cook, N.G.W., 1979. Fundamentals of Rock Mechanics, third ed. Chapman and Hall, London, 535 pp.

Kamb, W.B., 1959. Theory of preferred orientation developed by crystallization under stress. Journal of Geology 67, 153–170.

Kilsdonk, M.W., Wiltschko, D.V., 1988. Deformation mechanisms in the southeastern ramp region of the Pine Mountain block, Tennessee. Geological Society of America Bulletin 100, 653–664.

Lacazette, A., 1990. Application of linear elastic fracture mechanics to the quantitative evaluation of fluid inclusions decrepitation. Geology 18, 782–785.

Lacazette, A., Engelder, T., 1992. Fluid-driven cyclic propagation of a joint in the Ithaca Siltstone, Appalachian Basin, New York. In: Evans, B., Wong, T.-F. (Eds.), Fault Mechanics and Transport Properties of Rock. Academic Press, London, pp. 297–324.

Lamerson, P.R., 1982. The Fossil basin area and its relationship to the Absaroka thrust fault system. In: Powers, R.B. (Ed.), Geologic Studies of the Cordilleran Thrust Belt. Rocky Mountain Association of Geologists, pp. 279–340.

Mazzarini, F., Isola, I., 2007. Hydraulic connection and fluid overpressure in upper crustal rocks: Evidence from the geometry and spatial distribution of veins at Botrona quarry, southern Tuscany, Italy. Journal of Structural Geology 29, 1386–1399.

Meunier, J.D., 1989. Assessment of low-temperature fluid inclusions in calcite using microthermometry. Economic Geology 84, 167–170.

Mitra, G., Yonkee, W.A., Gentry, D.J., 1984. Solution cleavage and its relationship to major structures in the Idaho–Wyoming thrust belt. Geology 12, 354–358.

Montomoli, C., Ruggieri, G., Boiron, M.C., Cathelineau, M., 2001. Pressure fluctuation during uplift of the Northern Apennines (Italy): a fluid inclusion study. Tectonophysics 341, 121–139.

Montomoli, C., Ruggieri, G., Carosi, R., Dini, A., Genovesi, M., 2005. Fluid source and pressure-temperature conditions of high-salinity fluids in syn-tectonic veins from the Northeastern Apuan Alps (Northern Apennines, Italy). Physics and Chemistry of the Earth 30, 1005–1019.

Moore, J.C., et al., 1982. Offscraping and underthrusting of sediment at the deformation front of the Barbados Ridge: Deep Sea Drilling Project leg 78A. Geological Society of America Bulletin 93, 1065–1077.

Morse, J.W., Mackenzie, F.T., 1990. Geochemistry of Sedimentary Carbonates. Elsevier, 724 pp.

Nicholson, R., Pollard, D.D., 1985. Dilation and linkage of echelon cracks. Journal of Structural Geology 7 (5), 583–590.

O'Hara, K., Haak, A., 2002. A fluid inclusion study of fluid pressure and salinity variations in the footwall of the Rector Branch thrust, North Carolina, U.S.A. Journal of Structural Geology 14, 579–589.

Olson, J.E., Pollard, D.D., 1989. Inferring paleostresses from natural fracture patterns: A new method. Geology 17, 345–348.

Olson, J.E., Pollard, D.D., 1991. The initiation and growth of en echelon veins. Journal of Structural Geology 13 (5), 595–608.

Oriel, S.S., Platt, L.B., 1980. Geological map of the Preston $1^\circ \times 2^\circ$ quadrangle, southeastern Idaho and western Wyoming, scale 1:250,000. U.S. Geol. Surv. Misc. Geol. Invest. Map, 1–1127.

Oxburgh, E.R., Turcotte, D.L., 1974. Thermal gradients and regional metamorphism in overthrust terrains with special reference to the Eastern Alps. Schweizerische Mineralogische und Petrographische Mitteilungen 54, 641–662.

Parra, J.O., Collier, H.A., Angstman, B.G., 1999. Feasibility of detecting seismic waves between wells at the fractured Twin Creek Reservoir, Utah–Wyoming overthrust belt. In: Jordan, J.F. (Ed.), Reservoir Characterization; Recent Advances. AAPG Memoir. American Association of Petroleum Geologists, Vol. 71, Tulsa, OK, pp. 251–261.

Pollard, D.D., Aydin, A., 1988. Progress and understanding jointing over the past century. Geological Society of America Bulletin 100, 1181–1214.

Pollard, D.D., Segall, P., 1987. Theoretical displacements and stresses near fractures in rock, with applications of faults, joints, veins, dikes, and solution surfaces. In: Atkinson, B.K. (Ed.), Fracture Mechanics of Rock. Academic Press, London, pp. 277–349.

Pollard, D.D., Segall, P., Delaney, P.T., 1982. Formation and interpretation of dilatant echelon cracks. Geological Society of America Bulletin 93, 1291–1303.

Prezbindowski, D.R., Larese, R.E., 1987. Experimental stretching of fluid inclusions in calcite—Implications for diagenetic studies. Geology 15, 333–336.

Prokoph, A., Shields, G.A., Veizer, J., 2008. Compilation and time-series analysis of a marine carbonate delta O-18, delta C-13, Sr-87/Sr-86 and delta S-34 database through Earth history. Earth-Science Reviews 87, 113–133.

Roedder, E., 1984. Fluid Inclusions. Mineralogical Society of America Reviews in Mineralogy Vol. 12, 644.

Royse, F., Warner, M.A., Reese, D.L., 1975. Thrust belt structural geology and related stratigraphic problems Wyoming-Idaho-Northern Utah. In: Bolyard, D.W. (Ed.), Deep Drilling Frontiers of the Central Rocky Mountains Symposium. Rocky Mountain Association of Geologists, Denver, CO, pp. 41–54.

Rubey, W.W., 1973. Geologic map of the Afton quadrangle and part of the Big Piney quadrangle, Lincoln and Sublette Counties, Wyoming. U.S. Geological Survey Miscellaneous Geologic Investigations, Map I-686.

Rye, D.M., Bradbury, H.J., 1988. Fluid flow in the crust: an example from a Pyrenean thrust ramp. American Journal of Science 288, 197–235.

Segall, P., Pollard, D.D., 1983. Joint formation in granitic rock of the Sierra Nevada. Geological Society of America Bulletin 94, 563–575.

Shemesh, A., Ron, H., Erel, Y., Kolodny, Y., Nur, A., 1992. Isotopic composition of vein calcite and its fluid inclusions: Implications to paleohydrological systems, tectonic events and vein formation processes. Chemical Geology (Isotope Geoscience Section) 94, 307–314.

Smith, R.E., Wiltschko, D.V., 1996. Generation and maintenance of abnormal fluid pressures beneath a ramping thrust sheet;isotropic permeability experiments. Journal of Structural Geology 18, 951–970.

Sorkhabi, R., 2005. Geochemical signatures of fluid flow in thrust sheets: Fluid-inclusion and stable isotope studies of calcite veins in western Wyoming. In: Sorkhabi, R., Tsuji, Y. (Eds.), Faults, Fluid Flow, and Petroleum Traps. AAPG Memoir, 85, pp. 251–267.

Spang, J.H., Groshong Jr., R.H., 1981. Deformation mechanisms and strain history of a minor fold from the Appalachian Valley and Ridge province. Tectonophysics 72, 323–342.

Srivistava, D.G., Engelder, T., 1990. Crack-propagation sequence and pore-fluid conditions during fault-bend folding in the Appalachian Valley and Ridge, central Pennsylvania. Geological Society of America Bulletin 102, 116–128.

Suppe, J., Wittke, J.H., 1977. Abnormal pore-fluid pressures in relation to stratigraphy and structure in the active fold-and-thrust belt of northwestern Taiwan. Petroleum Geology of Taiwan 14, 11–24.

Teufel, L.W., 1980. Strain analysis of experimental superposed deformation using calcite twin lamellae. Tectonophysics 65, 291–309.

Teufelin, P., 1994. Closed-system veining during low-grade metamorphism, Rheems Quarry, Pennsylvania. Unpublished M.Sc. Thesis, University of Wisconsin, Madison, 66 pp.

Wanless, H.R., Belknap, R.L., Foster, H., 1955. Paleozoic and Mesozoic rocks of Gros Ventre, Teton, Hoback, and Snake River Ranges, Wyoming. Geological Society of America Memoir 63, 103.

Warner, M.A., Royse, F., 1987. Thrust faulting and hydrocarbon generation: Discussion. American Association of Petroleum Geologists Bulletin 71 (7), 882–889.

Wiltschko, D.V., Dorr, J.A., 1983. Timing and deformation in overthrust belt and foreland of Idaho, Wyoming, and Utah. American Association of Petroleum Geologists Bulletin 67, 1304–1322.

Yonkee, W.A., Parry, W.T., Bruhn, R.L., Cashman, P.H., 1989. Thermal models of thrust faulting: constraints from fluid-inclusion observations, Willard thrust-sheet, Idaho–Utah–Wyoming thrust belt. Geological Society of America Bulletin 101, 304–313.

Zhang, Y., Frantz, J.D., 1987. Determination of the homogenization temperatures and densities of supercritical fluids in the system NaCl-KCl-$CaCl_2$-H_2O using synthetic fluid inclusions. Chemical Geology 64, 335–350.